tapraid3/zpt-pt/zpt-pt/zpt00810/zpt9037d10z | xppws | S=1 | 5/15/10 | 1:17 | Art: 168070 | Input-KAF

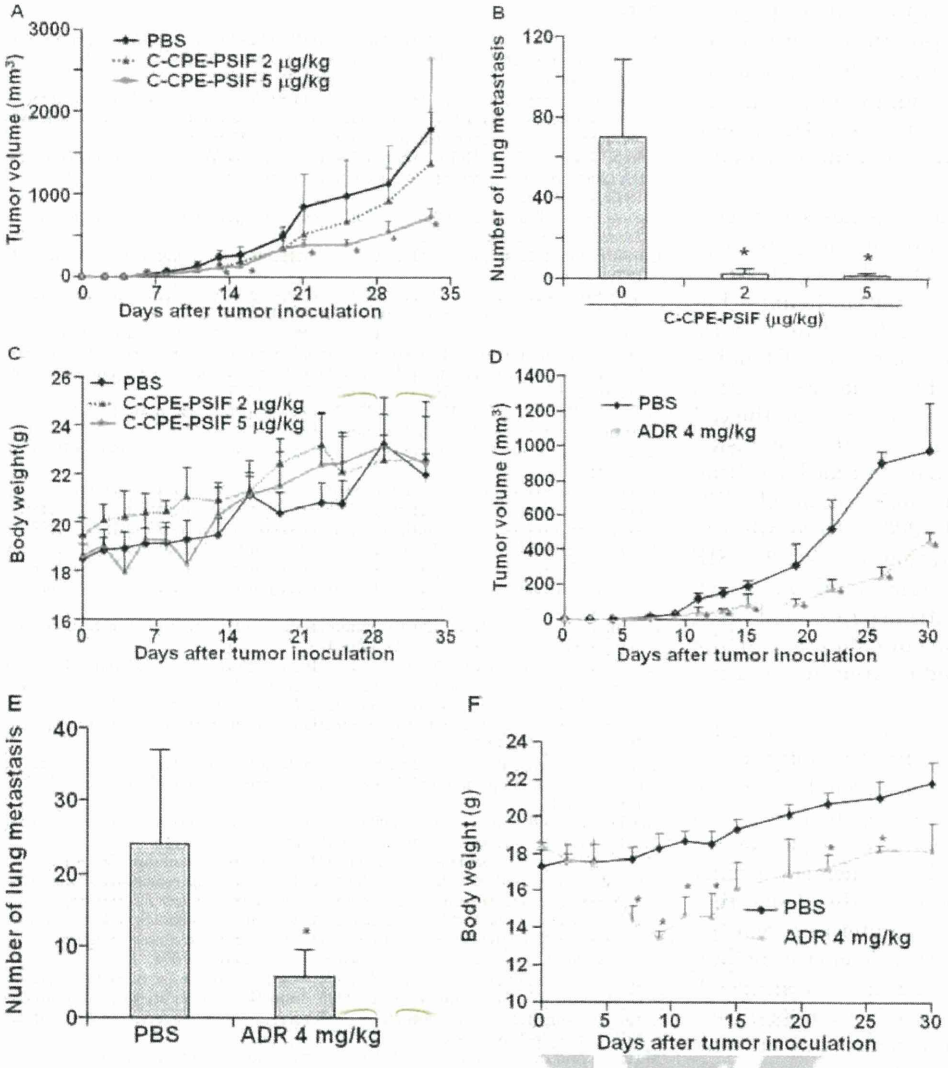

Fig. 3. Antitumor activity of C-CPE-PSIF for murine breast cancer 4T1 cells. 4T1 cells (1×10^5 cells) were intradermally inoculated into the right flanks of mice on day 0, and C-CPE-PSIF (A–C) or ADR (D–F) was intravenously injected three or two times a week at the indicated doses, respectively. Tumor volume (A and D) and body weight (B and E) were monitored. On day 35, the mice were sacrificed, their lungs were stained with India ink, and the number of spontaneous metastases was determined (C and F). Data are shown as means ± S.D. ($n = 5$). *, significantly different from the vehicle-treated group ($p < 0.01$). The data are representative of two independent experiments.

Although the in vitro metastasis activity of CL4-B16 cells was higher than that of parental B16 cells, the in vivo lung metastasis of CL4-B16 cells was lower than that of B16 cells. As shown in Supplemental Fig. 2, claudin-4 increased the invasiveness and migration activity of B16 cells in vitro and decreased lung metastasis in vivo. A possible explanation for this discrepancy might be the experimental model, which evaluates a different stage of metastasis. The migration and invasion activity involved in the early stage of metastasis was investigated in the in vitro analysis, whereas extravasation and colonization to an organ involved in the late stage of metastasis was evaluated by the in vivo experiment. The altered expression of claudin-4 changed the metastasis of 4T1 cells to the heart and liver, suggesting that claudin affects organ-specific metastasis (Erin et al., 2009). Claudin-4 might suppress the lung metastasis of B16 cells.

Claudin is a structural and functional component of TJs (Furuse and Tsukita, 2006). What is the role of claudin in metastasis? Metastasis is composed of three steps: leaving the primary site, entering the blood flow, and invading the distant site. In the first step, the combination of claudin members in the TJ strands may be important. The claudin family contains at least 24 members. Claudin is believed to form homo- and hetero-type claudin strands, and the pattern of the strands differs among tissues and determines the properties of TJ seals (Furuse and Tsukita, 2006). For example, rigid TJ seals were formed when claudin-11 or claudin-15 was exogenously expressed in Madin-Darby canine kidney cells, whereas the expression of claudin-11 or claudin-15 reduced the TJ integrity in LLC-PK1 cells by its dominant negative effects on TJ sealing (Van Itallie et al., 2003). Dominant negative effects of claudin-4 on the TJ barrier might contribute to an acceleration in the detachment of cancer cells from the primary tumor tissue. In the second and third steps of metastasis, cancer cells must move through the extracellular matrix at the primary site and the distant site. Cancer cells must degrade the extracellular matrix by the expression of matrix metalloproteinase and increase their motility. Claudin expression enhanced invasion with increased matrix metalloproteinase activity (Agarwal et al., 2005). There is a relationship between the levels of claudin-1/claudin-4 and the metastasis of human cancers, including hepatic, colonic, ovarian, and gastric cancers (Miwa et al., 2001; Agarwal et al., 2005; Resnick et al., 2005; Halder et al., 2008; Lee et al., 2008). The overexpression of claudin suppressed cancer metastasis in human pancreatic and gastric cancers (Michl et al., 2003; Mima et al., 2005; Ohtani et al., 2009). Claudin-4 suppressed or accelerated in vitro and in

AQ: D

AQ: E

vivo metastasis of human cancer cells (Agarwal et al., 2005; Ohtani et al., 2009). Cell–cell interaction through TJs regulates cell growth signaling (Matter et al., 2005). Taken together, these findings indicate that claudin family members might control several steps of cancer metastasis. The precise molecular mechanism and role of claudin in cancer metastasis remain to be determined.

Whether a claudin-4-targeting method causes severe side effects is critical for its clinical application in cancer therapy. Claudins play pivotal roles in TJ barrier and fence functions by maintaining cellular polarity in normal epithelium (Furuse and Tsukita, 2006). Claudins are believed to be more accessible in tumors than in normal epithelium. Claudins form TJ seals in lateral membranes between adjacent cells in normal epithelium, whereas claudins are exposed on the cell surface during tumorigenesis (Soler et al., 1999; Kominsky, 2006). Indeed, no local or systemic side effects have been observed after the intratumoral administration of CPE (Kominsky et al., 2007; Santin et al., 2007). Here, we also found that the systemic administration of C-CPE-PSIF causes no significant increase in biochemical markers (aspartate aminotransferase, alanine aminotransferase, and blood urea nitrogen) for toxicity at a therapeutic dose of 5 μg/kg (Supplemental Fig. 2). Thus, a claudin-targeting strategy might have weak side effects.

AQ: F

It is difficult to prepare recombinant claudin protein because of its hydrophobic property, and claudin has low antigenicity. Until recently, an antibody against the extracellular loop domain of claudin had never been successfully prepared, and C-CPE was the only known claudin binder. Recently, Romani et al. (2009) prepared a single-chain antibody fragment against claudin-3 by using phage display technology. They found that the antibody fragment binds to ovarian and uterine carcinoma cells in vitro. More importantly, a therapeutic monoclonal antibody against claudin-4 was developed. Suzuki et al. (2009) successfully prepared anticlaudin-4 antibody by immunizing claudin-4-expressing tumor cells into a mouse with autoimmune disease. The antibody mediates antibody-dependent cellular cytotoxicity and both in vitro and in vivo antitumor activity. Although the preparation of anticlaudin antibody may lead to a breakthrough in cancer therapy, the immunogenicity associated with immunotoxin clinical therapies is a future problem (Kreitman and Pastan, 2006). The C-terminal 30 amino acids are the minimum functional domain of C-CPE to bind to claudin-4 (Hanna et al., 1991). The C-terminal 30-amino-acid fragment was used to deliver a cytokine to claudin-4-expressing cells by genetic fusion (Yuan et al., 2009). Humanized antibody and the claudin-4-targeting peptide may be useful for cancer therapy in the near future.

In summary, this is the first report to indicate that systemic injection of a claudin-targeting molecule suppresses tumor growth and metastasis. Hematologic cells do not develop TJs; therefore, a claudin-targeting therapy may have no hematologic toxicity. We anticipate that claudin targeting will be a potent strategy for cancer therapy.

Acknowledgments

We thank members of our laboratory for useful comments and discussion and Drs. Y. Horiguchi (Osaka University, Osaka, Japan), S. Tsunoda (National Institute of Biomedical Innovation, Osaka, Japan), and M. Furuse (Kobe University, Hyogo, Japan) for providing C-CPE cDNA, PSIF cDNA, and claudin cDNA, respectively.

References

Agarwal R, D'Souza T, and Morin PJ (2005) Claudin-3 and claudin-4 expression in ovarian epithelial cells enhances invasion and is associated with increased matrix metalloproteinase-2 activity. *Cancer Res* **65:**7378–7385.

Dhawan P, Singh AB, Deane NG, No Y, Shiou SR, Schmidt C, Neff J, Washington MK, and Beauchamp RD (2005) Claudin-1 regulates cellular transformation and metastatic behavior in colon cancer. *J Clin Invest* **115:**1765–1776.

Erin N, Wang N, Xin P, Bui V, Weisz J, Barkan GA, Zhao W, Shearer D, and Clawson GA (2009) Altered gene expression in breast cancer liver metastases. *Int J Cancer* **124:**1503–1516.

Furuse M and Tsukita S (2006) Claudins in occluding junctions of humans and flies. *Trends Cell Biol* **16:**181–188.

Gupta GP and Massagué J (2006) Cancer metastasis: building a framework. *Cell* **127:**679–695.

Halder SK, Rachakonda G, Deane NG, and Datta PK (2008) Smad7 induces hepatic metastasis in colorectal cancer. *Br J Cancer* **99:**957–965.

Hanna PC, Mietzner TA, Schoolnik GK, and McClane BA (1991) Localization of the receptor-binding region of *Clostridium perfringens* enterotoxin using cloned toxin fragments and synthetic peptides. The 30 C-terminal amino acids define a functional binding region. *J Biol Chem* **266:**11037–11043.

Jemal A, Siegel R, Ward E, Hao Y, Xu J, Murray T, and Thun MJ (2008) Cancer statistics, 2008. *CA Cancer J Clin* **58:**71–96.

Kominsky SL (2006) Claudins: emerging targets for cancer therapy. *Expert Rev Mol Med* **8:**1–11.

Kominsky SL, Tyler B, Sosnowski J, Brady K, Doucet M, Nell D, Smedley JG 3rd, McClane B, Brem H, and Sukumar S (2007) *Clostridium perfringens* enterotoxin as a novel-targeted therapeutic for brain metastasis. *Cancer Res* **67:**7977–7982.

Kominsky SL, Vali M, Korz D, Gabig TG, Weitzman SA, Argani P, and Sukumar S (2004) *Clostridium perfringens* enterotoxin elicits rapid and specific cytolysis of breast carcinoma cells mediated through tight junction proteins claudin 3 and 4. *Am J Pathol* **164:**1627–1633.

Kreitman RJ and Pastan I (2006) Immunotoxins in the treatment of hematologic malignancies. *Curr Drug Targets* **7:**1301–1311.

Lee LY, Wu CM, Wang CC, Yu JS, Liang Y, Huang KH, Lo CH, and Hwang TL (2008) Expression of matrix metalloproteinases MMP-2 and MMP-9 in gastric cancer and their relation to claudin-4 expression. *Histol Histopathol* **23:**515–521.

Martin TA and Jiang WG (2001) Tight junctions and their role in cancer metastasis. *Histol Histopathol* **16:**1183–1195.

Matter K, Aijaz S, Tsapara A, and Balda MS (2005) Mammalian tight junctions in the regulation of epithelial differentiation and proliferation. *Curr Opin Cell Biol* **17:**453–458.

McClane BA and Chakrabarti G (2004) New insights into the cytotoxic mechanisms of *Clostridium perfringens* enterotoxin. *Anaerobe* **10:**107–114.

Michl P, Barth C, Buchholz M, Lerch MM, Rolke M, Holzmann KH, Menke A, Fensterer H, Giehl K, Löhr M, et al. (2003) Claudin-4 expression decreases invasiveness and metastatic potential of pancreatic cancer. *Cancer Res* **63:**6265–6271.

Michl P, Buchholz M, Rolke M, Kunsch S, Löhr M, McClane B, Tsukita S, Leder G, Adler G, and Gress TM (2001) Claudin-4: a new target for pancreatic cancer treatment using *Clostridium perfringens* enterotoxin. *Gastroenterology* **121:**678–684.

Mima S, Tsutsumi S, Ushijima H, Takeda M, Fukuda I, Yokomizo K, Suzuki K, Sano K, Nakanishi T, Tomisato W, et al. (2005) Induction of claudin-4 by nonsteroidal anti-inflammatory drugs and its contribution to their chemopreventive effect. *Cancer Res* **65:**1868–1876.

Mitic LL and Anderson JM (1998) Molecular architecture of tight junctions. *Annu Rev Physiol* **60:**121–142.

Morin PJ (2005) Claudin proteins in human cancer: promising new targets for diagnosis and therapy. *Cancer Res* **65:**9603–9606.

Morita K, Furuse M, Fujimoto K, and Tsukita S (1999) Claudin multigene family encoding four-transmembrane domain protein components of tight junction strands. *Proc Natl Acad Sci USA* **96:**511–516.

Mullin JM (1997) Potential interplay between luminal growth factors and increased tight junction permeability in epithelial carcinogenesis. *J Exp Zool* **279:**484–489.

Ohtani S, Terashima M, Satoh J, Soeta N, Saze Z, Kashimura S, Ohsuka F, Hoshino Y, Kogure M, and Gotoh M (2009) Expression of tight junction-associated proteins in human gastric cancer: down-regulation of claudin-4 correlates with tumor aggressiveness and survival. *Gastric Cancer* **12:**43–51.

Resnick MB, Konkin T, Routhier J, Sabo E, and Pricolo VE (2005) Claudin-1 is a strong prognostic indicator in stage II colonic cancer: a tissue microarray study. *Mod Pathol* **18:**511–518.

Romani C, Comper F, Bandiera E, Ravaggi A, Bignotti E, Tassi RA, Pecorelli S, and Santin AD (2009) Development and characterization of a human single-chain antibody fragment against claudin-3: a novel therapeutic target in ovarian and uterine carcinomas. *Am J Obstet Gynecol* **201:**70,e71–e79.

Saeki R, Kondoh M, Kakutani H, Tsunoda S, Mochizuki Y, Hamakubo T, Tsutsumi Y, Horiguchi Y, and Yagi K (2009) A novel tumor-targeted therapy using a claudin-4-targeting molecule. *Mol Pharmacol* **76:**918–926.

Saiki I (1997) Cell adhesion molecules and cancer metastasis. *Jpn J Pharmacol* **75:**215–242.

Santin AD, Bellone S, Marizzoni M, Palmieri M, Siegel ER, McKenney JK, Hennings L, Comper F, Bandiera E, and Pecorelli S (2007) Overexpression of claudin-3 and claudin-4 receptors in uterine serous papillary carcinoma: novel targets for a type-specific therapy using *Clostridium perfringens* enterotoxin (CPE). *Cancer* **109:**1312–1322.

Santin AD, Cané S, Bellone S, Palmieri M, Siegel ER, Thomas M, Roman JJ, Burnett A, Cannon MJ, and Pecorelli S (2005) Treatment of chemotherapy-resistant human ovarian cancer xenografts in C.B-17/SCID mice by intraperitoneal administration of *Clostridium perfringens* enterotoxin. *Cancer Res* **65:**4334–4342.

Soler AP, Miller RD, Laughlin KV, Carp NZ, Klurfeld DM, and Mullin JM (1999) Increased tight junctional permeability is associated with the development of colon cancer. *Carcinogenesis* **20:**1425–1431.

AQ: G Sonoda N, Furuse M, Sasaki H, Yonemura S, Katahira J, Horiguchi Y, and Tsukita S (1999) *Clostridium perfringens* enterotoxin fragment removes specific claudins from tight junction strands: Evidence for direct involvement of claudins in tight junction barrier. *J Cell Biol* **147:**195–204.

Staehelin LA (1973) Further observations on the fine structure of freeze-cleaved tight junctions. *J Cell Sci* **13:**763–786.

Steeg PS (2006) Tumor metastasis: mechanistic insights and clinical challenges. *Nat Med* **12:**895–904.

Suzuki M, Kato-Nakano M, Kawamoto S, Furuya A, Abe Y, Misaka H, Kimoto N, Nakamura K, Ohta S, and Ando H (2009) Therapeutic antitumor efficacy of monoclonal antibody against claudin-4 for pancreatic and ovarian cancers. *Cancer Sci* **100:**1623–1630.

Van Itallie CM, Fanning AS, and Anderson JM (2003) Reversal of charge selectivity in cation or anion-selective epithelial lines by expression of different claudins. *Am J Physiol Renal Physiol* **285:**F1078–F1084.

Vermeer PD, Einwalter LA, Moninger TO, Rokhlina T, Kern JA, Zabner J, and Welsh MJ (2003) Segregation of receptor and ligand regulates activation of epithelial growth factor receptor. *Nature* **422:**322–326.

Wodarz A and Näthke I (2007) Cell polarity in development and cancer. *Nat Cell Biol* **9:**1016–1024.

Wong CW, Song C, Grimes MM, Fu W, Dewhirst MW, Muschel RJ, and Al-Mehdi AB (2002) Intravascular location of breast cancer cells after spontaneous metastasis to the lung. *Am J Pathol* **161:**749–753.

Yuan X, Lin X, Manorek G, Kanatani I, Cheung LH, Rosenblum MG, and Howell SB (2009) Recombinant CPE fused to tumor necrosis factor targets human ovarian cancer cells expressing the claudin-3 and claudin-4 receptors. *Mol Cancer Ther* **8:**1906–1915.

Address correspondence to: Dr. Masuo Kondoh, Laboratory of Bio-Functional Molecular Chemistry, Graduate School of Pharmaceutical Sciences, Osaka University, Suita, Osaka 565-0871, Japan. E-mail: masuo@phs.osaka-u.ac.jp AQ: H

OPEN ACCESS Freely available online

PLoS one

A Novel Screening System for Claudin Binder Using Baculoviral Display

Hideki Kakutani[1☯], Azusa Takahashi[1☯], Masuo Kondoh[1*], Yumiko Saito[1], Toshiaki Yamaura[1], Toshiko Sakihama[2], Takao Hamakubo[2], Kiyohito Yagi[1*]

1 Laboratory of Bio-Functional Molecular Chemistry, Graduate School of Pharmaceutical Sciences, Osaka University, Suita, Osaka, Japan, **2** Department of Molecular Biology and Medicine, Research Center for Advanced Science and Technology, The University of Tokyo, Meguro, Tokyo, Japan

Abstract

Recent progress in cell biology has provided new insight into the claudin (CL) family of integral membrane proteins, which contains more than 20 members, as a target for pharmaceutical therapy. Few ligands for CL have been identified because it is difficult to prepare CL in an intact form. In the present study, we developed a method to screen for CL binders by using the budded baculovirus (BV) display system. CL4-displaying BV interacted with a CL4 binder, the C-terminal fragment of *Clostridium perfringens* enterotoxin (C-CPE), but it did not interact with C-CPE that was mutated in its CL4-binding region. C-CPE did not interact with BV and CL1-displaying BV. We used CL4-displaying BV to select CL4-binding phage in a mixture of a scFv-phage and C-CPE-phage. The percentage of C-CPE-phage in the phage mixture increased from 16.7% before selection to 92% after selection, indicating that CL-displaying BV may be useful for the selection of CL binders. We prepared a C-CPE phage library by mutating the functional amino acids. We screened the library for CL4 binders by affinity to CL4-displaying BV, and we found that the novel CL4 binders modulated the tight-junction barrier. These findings indicate that the CL-displaying BV system may be a promising method to produce a novel CL binder and modulator.

Citation: Kakutani H, Takahashi A, Kondoh M, Saito Y, Yamaura T, et al. (2011) A Novel Screening System for Claudin Binder Using Baculoviral Display. PLoS ONE 6(2): e16611. doi:10.1371/journal.pone.0016611

Editor: Vladimir Uversky, University of South Florida College of Medicine, United States of America

Received November 22, 2010; **Accepted** December 24, 2010; **Published** February 14, 2011

Funding: This work was supported by a Grant-in-Aid for Scientific Research from the Ministry of Education, Culture, Sports, Science and Technology, Japan (21689006), by a Health and Labor Sciences Research Grant from the Ministry of Health, Labor and Welfare of Japan, by Takeda Science Foundation, by a Suzuken Memorial Foundation, by a grant from Kansai Biomedical Cluster project in Saito, which is promoted by the Knowledge Cluster Initiative of the Ministry of Education, Culture, Sports, Science and Technology, Japan and by a Research Grant for Promoting Technological Seeds from Japan Science and Technology Agency. A.T. is supported by Research Fellowships of the Japan Society for the Promotion of Science for Young Scientists. The funders had no role in study design, data collection and analysis, decision to publish, or preparation of the manuscript.

Competing Interests: The authors have declared that no competing interests exist.

* E-mail: masuo@phs.osaka-u.ac.jp (MK); yagi@phs.osaka-u.ac.jp (KY)

☯ These authors contributed equally to this work.

Introduction

Tight junctions (TJ) are intercellular adhesion complexes in epithelial and endothelial cells; TJs are located in the most apical part of the complexes [1]. TJs have a barrier function and a fence function [2–4]. TJs contribute to epithelial and endothelial barrier functions by restricting the diffusion of solutes through the paracellular pathway. TJs maintain cellular polarity by preventing the free movement of membrane proteins between the apical and basal membranes [5]. Loss of cell-cell adhesion and cellular polarity commonly occurs in the early stages of cancer [6]. Modulation of the TJ barrier function can be a method to enhance drug absorption, and TJ components exposed on the surface of cancer cells can be a target for cancer therapy.

Biochemical analyses of TJs have identified TJ components, such as occludin, claudins (CLs) and junction adhesion molecule [7]. The CL family contains more than 20 integral tetra-transmembrane proteins that play pivotal roles in the TJ barrier and fence functions. CL1-deficient mice lack the epidermal barrier, while CL5-deficient mice lack the blood-brain barrier [8,9], indicating that the regulation of the TJ barrier by modulation of CLs may be a promising method for drug delivery. *Clostridium perfringens* enterotoxin (CPE) causes food poisoning in humans [10]. An interaction between the C-terminal domain of CPE (C-CPE) with CL4 deregulates the TJ barrier [11,12]. We previously found that C-CPE enhances jejunal absorption through its interaction with CL4, indicating that a CL binder is a potent drug-delivery system [13].

The majority of lethal cancers are derived from epithelial tissues [14]. Malignant tumor cells frequently exhibit abnormal TJ function, followed by the deregulation of cellular polarity and intercellular contact, which is commonly observed in both advanced tumors and the early stages of carcinogenesis [6]. Some CLs are overexpressed in various types of cancers. For example, CL3 and CL4 are overexpressed in breast, prostate, ovarian, pancreatic and gastric cancers. CL1, CL7, CL10 and CL16 are overexpressed in colon, gastric, thyroid and ovarian cancers, respectively [15,16]. These findings indicate that the CLs may be a target molecule for cancer therapy. A receptor for CPE is CL4 [11,12]. CPE has anti-tumor activity against human pancreatic and ovarian cancers without side effects [17,18]. The CLs binders will be useful for cancer-targeting therapy.

As above, recent investigations of CLs provide new insight into their use as pharmaceutical agents; for example, a CL binder may be used in drug delivery and anti-tumor therapy. Selection of a CL binder by using a recombinant CL protein is a putative method to

prepare a CL binder. However, CLs are four-transmembrane proteins with high hydrophobicity; there has been little success in the preparation of intact CL protein. Recently, a novel type of protein expression system that uses baculovirus has been developed. Membrane proteins are displayed on the budded baculovirus (BV) in their active form [19–21], indicating that the BV system may be useful for the preparation of a CL binder. In the present study, we investigated whether a CL binder was screened by using a CL-displaying BV.

Results

Preparation of CL4-displaying BV

C-CPE is the only known CL binder and modulator [12,13,22]. C-CPE has affinity to CL4 in a nanomolar range [23]. We chose C-CPE and CL4 as models of the CL binder and CL, respectively. Several reports indicate that membrane proteins expressed on the surface of BV are in an intact form [19–21]. To check the expression of CL4 on the BV, we performed immunoblot analysis of the lysate of CL4-BV against CL4. As shown in Fig. 1A, CL4 was detected in the virus lysates. To determine if the CL4 expressed on the virus has an intact form, we performed enzyme-linked immunosorbent assay (ELISA) with CL4-BV-coated immunoplates. C-CPE binds to the extracellular loop domain of CL4 [23]. After the addition of C-CPE to the CL4-BV-coated plate, the C-CPE bound to the CL4-BV-coated plate was detected by anti-his-tag antibody, followed by incubation with horseradish peroxidase-labeled antibody. C-CPE was dose-dependently bound to CL4-BV, whereas C-CPE did not interact with wild-BV (Fig. 1B). Deletion of the CL4-binding region (C-CPE303) attenuated the interaction of C-CPE with CL4-BV (Fig. 1C). Together, these results indicate that the CL4 displayed on BV may have an intact extracellular loop region.

Selection of C-CPE-phage by using CL4-BV

We next examined the interaction between C-CPE-phage and CL4-BV. As shown in Fig. 2A, C-CPE-phage bound to CL4-BV but not to wild-BV, and a scFv-phage did not bind to CL4-BV. To determine if CL-BV can be used to select CL binders, we prepared a mixture of C-CPE-phage and scFv-phage at a ratio of 2:10 and used CL4-BV to select CL4-binding phage in the mixtures. The amount of C-CPE-phage was increased to 11 of 12 clones in the mixture (Fig. 2B), indicating that CL-BV may be useful in the preparation of CL binders.

We previously found that each substitution of S304, S305, S307, N309, S313 and K318 with alanine increased the binding of C-CPE to CL4 [24]. Here, we prepared a phage library for C-CPE by randomly changing the functional 6 amino acids to any of the 20 amino acids. To confirm the diversity of the library, we checked the sequences of 17 randomly isolated clones. Each of the 17 clones had a different sequence, indicating that the library has a diverse population of C-CPE mutants (Table 1).

Then, we screened the CL4-binding phage by their affinity to CL4-BV. After addition of the C-CPE library to CL4-BV-adsorbed tubes, the CL4-BV-bound phages were recovered (1st screening). We repeated this screening process two more times (2nd screening and 3rd screening). If the number of CL4-bound phage is increased during the screening, the ratio of the incubated phage titers to the recovered phage titers will increase. As shown in Fig. 3A, the ratio was increased during screening from 4.5×10^{-7} to 5.5×10^{-5}, indicating that the screening system for CL4 binders may work. Indeed, the number of monoclonal phage clones with high affinity to CL4-BV was increased after the 3rd screening compared with that after the 2nd screening (Fig. 3B).

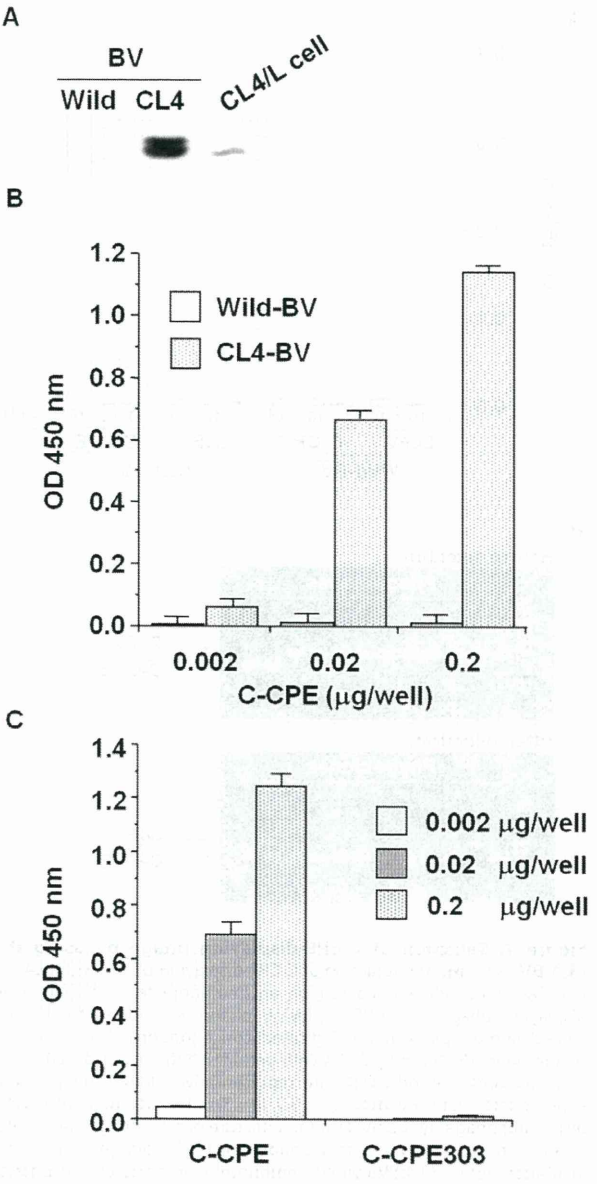

Figure 1. Preparation of CL4-displaying BV. A) Immunoblot analysis. Wild-BV and CL4-BV (0.1 μg/lane) were subjected to SDS-PAGE, followed by immunoblot analysis with anti-CL4 antibody. The lysate of CL4-expressing L (CL4/L) cells was used as a positive control. B, C) Interaction of a CL4 binder with CL4-BV. Immunotubes were coated with the wild-BV or CL4-BV, and C-CPE (B) or mutated C-CPE (C) was added to the BV-coated immunotubes at the indicated concentration. C-CPE bound to the BV-coated tubes was detected by ELISA with an anti-his-tag antibody.
doi:10.1371/journal.pone.0016611.g001

We analyzed the sequences of the CL4-BV-bound phages and got novel CL4-binder candidates with amino acid sequences that differed from the wild-type sequence (Table 2). To investigate their CL4-binding, we prepared the recombinant proteins of the binders and investigated their interaction with CL4 by ELISA with CL-BVs. As shown in Fig. 4A, the novel C-CPE derivatives had affinity to CL4 but not CL1. Next, we investigated whether the novel CL4 binders modulate TJ barrier in Caco-2 monolayer cell sheets, a popular model for the evaluation of TJ barriers [25].

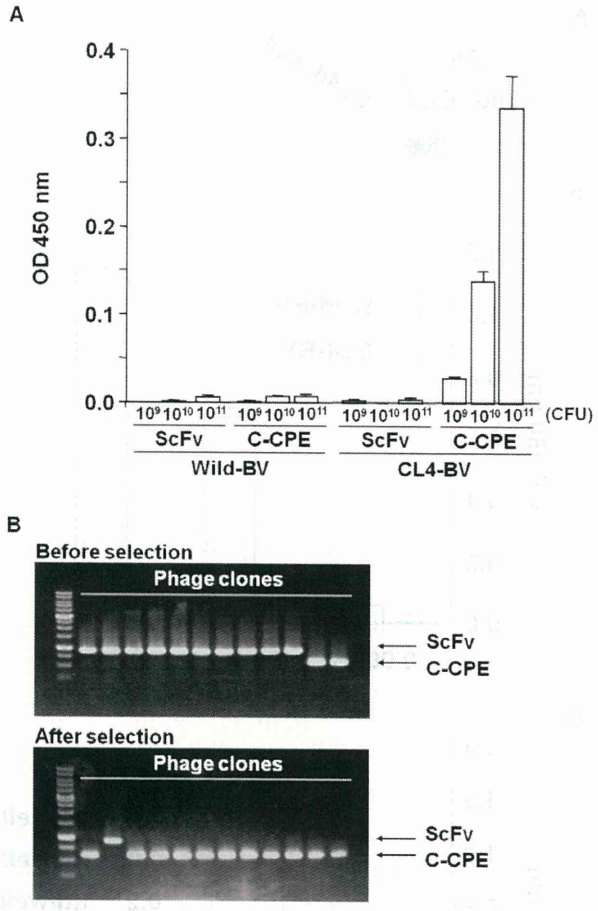

Figure 2. Selection of C-CPE-displaying phage by using the CL4-BV system. A) Interaction of C-CPE-displaying phage with CL4-BV. Wild-BV or CL4-BV was coated on an immunoplate, and then scFv-displaying phage or C-CPE-displaying phage was added to the BV-coated immunoplate at the indicated concentrations. The BV-bound phages were detected by ELISA with anti-M13 antibody as described in Materials and methods. Data are representative of two independent experiments. Data are means ± SD (n = 3). B) Enrichment of C-CPE-displaying phage by the BV system. A mixture of scFv-phage and C-CPE-phage (mixing ratio of scFv-phage to C-CPE-phage = 2:10) was incubated with a CL4-BV-coated immunotube, and the bound phages were recovered. Each phage clone was identified by PCR amplification, followed by agarose gel electrophoresis. Upper and lower pictures are before and after the selection, respectively. The putative sizes of the PCR products are 856 and 523 bp in scFv and C-CPE, respectively. The data are representative of two independent experiments.
doi:10.1371/journal.pone.0016611.g002

Treatment of the cells with C-CPE resulted in decreased transepithelial electrical resistance (TEER) values, a marker of TJ integrity, and the TEER values increased after removal of C-CPE. The C-CPE derivatives (clones 1–5) had TJ-modulating activity similar to that of C-CPE (Fig. 4B).

Discussion

CL is a promising target for pharmaceutical therapy. However, CL has low antigenicity, and there has been little success in the preparation of monoclonal antibody against the extracellular loop region of CL. The three-dimensional structure of CL has never been determined, so it is impossible to perform a theoretical design of a CL binder based on the structural information. In the present study, we developed a novel screening system for CL binders by using a BV system and a C-CPE phage display library, and we used this system to identify novel CL4 binders.

Table 1. C-CPE phage library.

	304	305	307	309	313	318
C-CPE	**S**	**S**	**S**	**N**	**S**	**K**
Clone 1	V	T	C	V	N	K
2	C	P	A	H	L	T
3	A	G	G	V	P	P
4	R	G	H	L	E	H
5	A	A	P	S	R	Q
6	P	A	P	D	P	A
7	C	T	T	T	N	K
8	H	P	S	P	G	H
9	R	G	G	R	N	R
10	A	P	S	T	Q	P
11	V	L	G	N	M	R
12	P	P	A	T	F	R
13	G	D	C	S	N	L
14	F	R	V	F	R	N
15	S	Q	Q	W	T	T
16	S	R	L	E	W	Q
17	K	R	E	R	Q	S

Phage clones were randomly picked up from the C-CPE phage library, and the amino acids sequences of C-CPE mutant were analyzed.
doi:10.1371/journal.pone.0016611.t001

In ligand screening, the preparation of a receptor for the ligand is very critical. Membrane proteins are especially difficult to prepare as recombinant protein with an intact structure. Functional membrane proteins such as cell-surface proteins are heterologously expressed on BV in their native forms [19–21]. Interactions between membrane proteins can be detected by using receptor-displaying and ligand-displaying BV [21]. In the present report, we found that CL4-BV interacts with a CL4 binder, C-CPE, but it does not interact with C-CPE303 that lacks the CL4-binding residues of C-CPE. The CL4-binding site of C-CPE corresponds to that of CPE; so, the second extracellular loop of CL appears to be the C-CPE-binding site [23,26]. These findings indicate that CL4 displayed on BV may have native form. We anticipate that CL-BV will be useful for the preparation of CL binders, such as peptides and antibodies.

To the best of our knowledge, the preparation of CL binder has been performed by only four groups. Offner et al. prepared polyclonal antibodies against extracellular domains of CL3 and CL4 [27], Ling et al. screened peptide types of CL4 binder by using a 12-mer peptide phage display library and CL4-expressing cells [28], Suzuki et al. generated a monoclonal antibody against the second extracellular loop of CL4 from mice immunized with a human pancreatic cancer cell line [29] and Romani et al. screened scFv against CL3 by using a human antibody phage display library [30]. However, the CL modulators have never been developed; thus, C-CPE is the only known CL4 modulator [12]. In the present study, we prepared a C-CPE phage library containing C-CPE mutants in which each of the 6 functional amino acids was randomly replaced with an amino acid, and we isolated CL4 binders by using CL4-BV as a screening ligand. Interestingly, all of

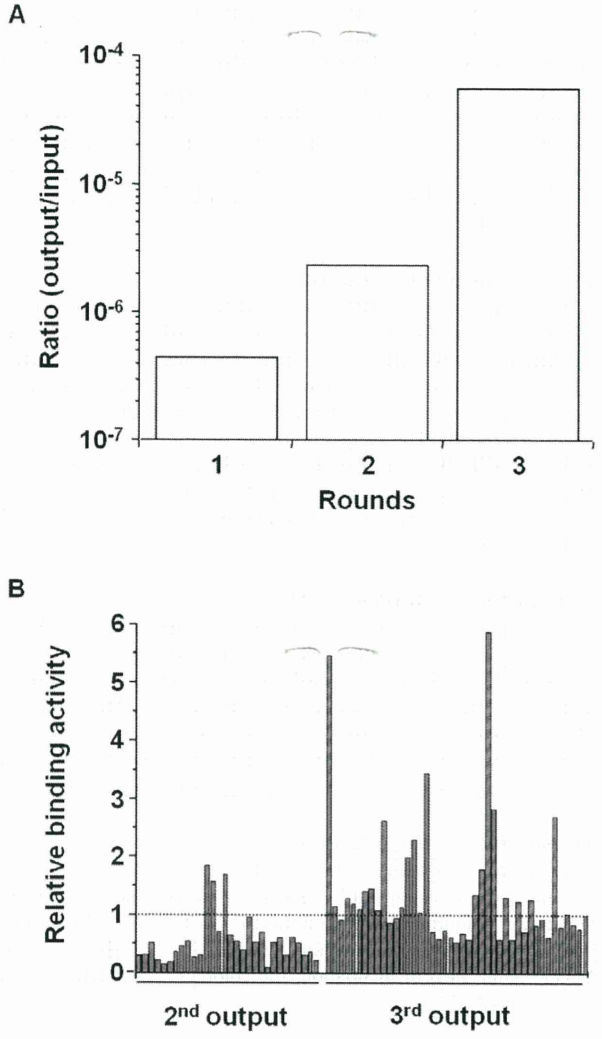

Figure 3. Screening of a novel CL4 binder. A) Enrichment of phages with affinity to CL4-BV. CL4-BVs coated on immunotubes were incubated with the C-CPE-derivative phage library at 1.6×10^{12} CFU titer (1^{st} input phage). The phages bound to CL4-BV were recovered (1^{st} output phage). The CL4-BV-binding phages were subjected to two additional cycles of the incubation and wash step, resulting in 2^{nd}, 3^{rd} output phage. The ratio of output phage to input phage titers was calculated. B) Monoclonal analysis of C-CPE-derivative phage. CL4-BV-bound phage clones were isolated from the 2^{nd} and 3^{rd} output phages, and the interaction of the monoclonal phage with CL4-BV was examined by ELISA with anti-M13 antibody as described in Materials and methods. Data are expressed as relative binding to that of C-CPE-phage indicated by the most right column.
doi:10.1371/journal.pone.0016611.g003

the CL4 binders modulated TJ barriers. We are investigating why the substitution of the amino acids with the other amino acids modulated CL4. These findings indicate that a BV screening system with a C-CPE library may be a powerful method to develop CL modulators.

The CL family forms various types of TJ barriers through combinations of its more than 20 members in homophilic/heterophilic CL strands [31,32]. Intercellular proteins ZO-1 and ZO-2 determine the localization of CL strands [33]. If a screening system to reconstitute heterogeneous CL strands with ZO-1 and/or ZO-2 is developed, then useful and effective CL modulators can be identified. In this point, the BV system has extremely superior features. G protein and G protein-coupled receptors have been

Table 2. CL4-binding phages.

	304	305	307	309	313	318
C-CPE	**S**	**S**	**S**	**N**	**S**	**K**
Clone 1	R	V	S	A	R	R
2	R	S	V	A	R	K
3	G	D	G	R	T	R
4	S	A	P	R	S	A
5	R	S	L	K	S	K

The sequences of C-CPE mutant in the CL4-binding phages were analyzed.
doi:10.1371/journal.pone.0016611.t002

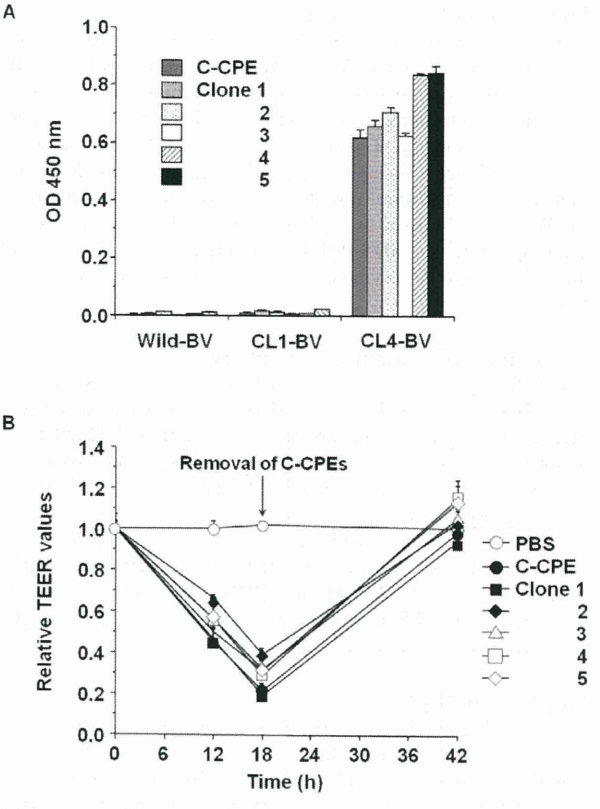

Figure 4. Isolation of a novel CL4 modulator. A) Interaction of the C-CPE derivatives with CL4. C-CPE derivatives were prepared as his-tagged recombinant proteins. The C-CPE derivatives (0.02 μg) were added to CL-BV-coated immunoplates, followed by detection of the C-CPE derivatives bound to CL-BV. Data are means ± SD (n = 4). B) Modulation of tight junction-barriers. Caco-2 cells were cultured on Transwell™ chambers. When TEER values reach a plateau, the cells were treated with C-CPE or C-CPE derivatives at the indicated concentrations. After 18 h of exposure to the C-CPEs, the cells were washed with medium to remove C-CPEs, and then the cells were cultured for an additional 24 h. Changes in TEER values were monitored during the C-CPEs treatment. Relative TEER values were calculated as the ratio of TEER values at 0 h. Data are representative of two independent experiments. The data are means ± SD (n = 4).
doi:10.1371/journal.pone.0016611.g004

functionally reconstituted in BV [20,34], and functional γ-secretase complexes have also been reconstituted on BV [35]. In the near future, the reconstituted CL system on BV will be developed and used for the screening of CL binders and modulators, hopefully leading to breakthroughs in pharmaceutical therapies that target CLs.

Materials and Methods

Recombinant BV construction and Sf9 cell culture

Recombinant BV was prepared by using the Bac-to-Bac expression system, according to the manufacturer's instructions (Invitrogen, Gaithersburg, MD). Briefly, mouse CL1 and CL4 cDNA (kind gifts from Dr. M Furuse, Kobe University, Japan) were inserted into pFastBac1, and the resulting plasmids were transduced into DH10Bac *E. Coli* cells. Recombinant bacmid DNA was extracted from the cells. Sf9 cells were transduced with the bacmid coding CL, and the recombinant BV was recovered by centrifugation of the conditioned medium [36].

Preparation of the BV fractions

Sf9 cells (2×10^6 cells) were infected with recombinant BV at a multiplicity of infection of 5. Seventy-two hours after infection, the BV fraction was recovered from the culture supernatant of infected Sf9 cells by centrifugation. The pellets of the BV fraction were resuspended in Tris-buffered saline (TBS) containing 1% protease inhibitor cocktail (Sigma-Aldrich, St. Louis, MO) and then stored at 4°C until use. The expression of CL1 and CL4 in the BV was confirmed by sodium dodecyl sulfate-polyacrylamide gel electrophoresis (SDS-PAGE) and immunoblot analysis with anti-CL antibodies (Zymed Laboratory, South San Francisco, CA).

Preparation of mutant C-CPE library

C-CPE fragments in which the functional amino acids (S304, S305, S307, N309, S313 and K318) [24] were randomly mutated were prepared by polymerase chain reaction (PCR) with pET-H_{10}PER as a template, a forward primer (5′-catgccatggccgatatagaaaaagaaatccttgatttagctgctg-3′, Nco I site is underlined) and a reverse primer (5′-ttttccttttgcggccgcaaa*snn*ttgaaataatat*snn*ataagggta*snn*tcc*snn*ata*snnsnn*attagcttt-3′, Not I site is underlined, and the randomly mutated amino acids are in italics). The PCR fragments were inserted into a pY03 phagemid at the NcoI/NotI sites [22]. The resultant phagemid containing the C-CPE mutant library was transduced into *E. coli* TG1 cells, and then the cells were stored at −80°C.

Preparation of phage

TG1 cells containing phagemid coding a scFv, C-CPE, C-CPE mutant or C-CPE mutant library were culture in 2YT medium containing 2% glucose and ampicillin. When the cells grew to a growing phage, M13K07 helper phages (Invitrogen) were added, and the medium was changed into 2YT medium containing ampicillin and kanamycin. After an additional 6 h of culture, the phages in the conditioned medium were precipitated with polyethylene glycol. The phages were suspended in phosphate-buffered saline (PBS) and stored at 4°C until use.

ELISA

Wild-BVs or CL-BVs (0.5 μg/well) were adsorbed onto an immunoplate (Greiner Bio-One, Frickenhausen, Germany). The wells were washed with PBS and blocked with TBS containing 1.6% BlockAce (Dainippon Sumitomo Pharma, Osaka, Japan). C-CPEs or phages were incubated in the immunoplate, and the BV-bound C-CPEs or phages were detected by using anti-his-tag antibody (Novagen, Darmstadt, Germany) or anti-M13 antibody (Amersham-Pharmacia Biotech, Uppsala, Sweden), respectively, horseradish peroxidase-labelled secondary antibody and TMB peroxidase substrate (Nacalai Tesque, Kyoto, Japan). The immunoreactive C-CPEs or phages were quantified by the measurement of absorbance at 450 nm. In the screening of phages, the data were normalized by the amounts of phages, which were quantified by ELISA for the FLAG-tag contained in the coat protein.

Selection of phage by using BV

A total of 0.5 μg of BV was adsorbed onto an immunotube (Nunc, Roskilde, Denmark). The tube was washed with PBS and blocked with TBS containing 4.0% BlockAce. The BV-coated tubes were incubated with mixture of phages, and then the tubes were washed 15 times with PBS and 15 times with PBS containing 0.05% Tween 20. The phages bound to the tube were eluted with 100 mM HCl. TG1 cells were infected with the eluted phages, and phages were prepared as described above. The resulting phages were subjected to repeated selection by using the BV-coated immunotubes.

Identification of a phage clone

To identify an isolated phage clone, we performed PCR or sequencing analysis. We amplified the inserted fragment into the phagemid by PCR using forward primer 5′-caggaaacagctatgac-3′ and reverse primer 5′-gtaaatgaattttctgtatgagg-3′. The resultant PCR products were subjected to agarose gel electrophoresis followed by staining with ethidium bromide. We performed a sequence analysis with primer 5′-gtaaatgaattttctgtatgagg-3′.

Measurement of phage titer

To quantify the concentration of phages, we measured the titer (colony formation unit (CFU)/ml) of the phage solution. Briefly, the phage solution was diluted to 10^{-5}–10^{-10} with PBS. The diluted solution was seeded onto Petrifilm™ (Tech-Jam, Osaka, Japan). After 24 h of incubation, the colonies were counted, and the titer was calculated.

Purification of C-CPE mutants

C-CPE and C-CPE303, in which the CL-4 binding region of C-CPE was deleted, were prepared as described previously [13]. To prepare plasmid containing C-CPE mutants, the C-CPE mutant fragment was PCR-amplified by using phagemids coding C-CPE mutants as a template. The resulting PCR fragment was inserted into pET16b, and the sequence was confirmed. The plasmids were transduced into *E. coli* strain BL21 (DE3), and production of mutant C-CPEs was induced by the addition of isopropyl-D-thiogalactopyranoside. The harvested cells were lysed in buffer A (10 mM Tris-HCl, pH 8.0, 400 mM NaCl, 5 mM $MgCl_2$, 0.1 mM phenylmethanesulfonyl fluoride, 1 mM 2-mercaptoethanol, and 10% glycerol) that was supplemented with 8 M urea when necessary. The lysates were applied to HiTrap™ Chelating HP (GE Healthcare, Buckinghamshire, UK), and mutant C-CPEs were eluted with buffer A containing 100–400 mM imidazole. The buffer was exchanged with PBS by using a PD-10 column (GE Healthcare), and the purified protein was stored at −80°C until use. Purification of the mutant C-CPEs was confirmed by SDS-PAGE, followed by staining with Coomassie Brilliant Blue and by immunoblotting with anti-his-tag antibody (Novagen). Protein was quantified by using a BCA protein assay kit with bovine serum albumin as a standard (Pierce Chemical, Rockford, IL).

TEER assay

Caco-2 cells were seeded in Transwell^{TM} chambers (Corning, NY) at a subconfluent density. The TEER of the Caco-2 monolayer cell sheets on the chamber was monitored by using a Millicell-ERS epithelial volt-ohmmeter (Millipore, Billerica, MA). When TEER values reached a plateau, indicating that TJs were well-developed in the cell sheets, the Caco-2 monolayers were treated with C-CPE or C-CPE mutants on the basal side of the chamber. Changes in TEER values were monitored. The TEER values were normalized by the area of the Caco-2 monolayer, and the TEER value of a blank Transwell^{TM} chamber (background) was subtracted.

Acknowledgments

We thank Drs. S. Tsunoda (National Institute of Biomedical Innovation, Japan), Y. Tsutsumi, Y. Mukai (Osaka University, Japan) for their kind instruction of phage display technology. We also thank Drs. Y. Horiguchi (Osaka University, Japan), S. Tsukita (Kyoto University, Japan) and members of our laboratory for providing us C-CPE cDNA, CL-expressing cells and their useful comments and discussion, respectively.

Author Contributions

Conceived and designed the experiments: MK TS TH KY. Performed the experiments: HK AT MK YS TY TS. Analyzed the data: HK AT MK KY. Contributed reagents/materials/analysis tools: HK AK TS TH. Wrote the manuscript: HK MK TY.

References

1. Farquhar MG, Palade GE (1963) Junctional complexes in various epithelia. J Cell Biol 17: 375–412.
2. Anderson JM, Van Itallie CM, Fanning AS (2004) Setting up a selective barrier at the apical junction complex. Curr Opin Cell Biol 16: 140–145.
3. Balda MS, Matter K (1998) Tight junctions. J Cell Sci 111(Pt 5): 541–547.
4. Tsukita S, Furuse M, Itoh M (2001) Multifunctional strands in tight junctions. Nat Rev Mol Cell Biol 2: 285–293.
5. Mitic LL, Anderson JM (1998) Molecular architecture of tight junctions. Annu Rev Physiol 60: 121–142.
6. Wodarz A, Nathke I (2007) Cell polarity in development and cancer. Nat Cell Biol 9: 1016–1024.
7. Schneeberger EE, Lynch RD (2004) The tight junction: a multifunctional complex. Am J Physiol 286: C1213–C1228.
8. Furuse M, Hata M, Furuse K, Yoshida Y, Haratake A, et al. (2002) Claudin-based tight junctions are crucial for the mammalian epidermal barrier: a lesson from claudin-1-deficient mice. J Cell Biol 156: 1099–1111.
9. Nitta T, Hata M, Gotoh S, Seo Y, Sasaki H, et al. (2003) Size-selective loosening of the blood-brain barrier in claudin-5-deficient mice. J Cell Biol 161: 653–660.
10. McClane BA (1994) *Clostridium perfringens* enterotoxin acts by producing small molecule permeability alterations in plasma membranes. Toxicology 87: 43–67.
11. Katahira J, Inoue N, Horiguchi Y, Matsuda M, Sugimoto N (1997) Molecular cloning and functional characterization of the receptor for *Clostridium perfringens* enterotoxin. J Cell Biol 136: 1239–1247.
12. Sonoda N, Furuse M, Sasaki H, Yonemura S, Katahira J, et al. (1999) *Clostridium perfringens* enterotoxin fragment removes specific claudins from tight junction strands: Evidence for direct involvement of claudins in tight junction barrier. J Cell Biol 147: 195–204.
13. Kondoh M, Masuyama A, Takahashi A, Asano N, Mizuguchi H, et al. (2005) A novel strategy for the enhancement of drug absorption using a claudin modulator. Mol Pharmacol 67: 749–756.
14. Jemal A, Siegel R, Ward E, Hao Y, Xu J, et al. (2008) Cancer statistics, 2008. CA Cancer J Clin 58: 71–96.
15. Kominsky SL (2006) Claudins: emerging targets for cancer therapy. Expert Rev Mol Med 8: 1–11.
16. Morin PJ (2005) Claudin proteins in human cancer: promising new targets for diagnosis and therapy. Cancer Res 65: 9603–9606.
17. Michl P, Buchholz M, Rolke M, Kunsch S, Lohr M, et al. (2001) Claudin-4: a new target for pancreatic cancer treatment using *Clostridium perfringens* enterotoxin. Gastroenterology 121: 678–684.
18. Santin AD, Cane S, Bellone S, Palmieri M, Siegel ER, et al. (2005) Treatment of chemotherapy-resistant human ovarian cancer xenografts in C.B-17/SCID mice by intraperitoneal administration of *Clostridium perfringens* enterotoxin. Cancer Res 65: 4334–4342.
19. Loisel TP, Ansanay H, St-Onge S, Gay B, Boulanger P, et al. (1997) Recovery of homogeneous and functional beta 2-adrenergic receptors from extracellular baculovirus particles. Nat Biotechnol 15: 1300–1304.
20. Sakihama T, Masuda K, Sato T, Doi T, Kodama T, et al. (2008) Functional reconstitution of G-protein-coupled receptor-mediated adenylyl cyclase activation by a baculoviral co-display system. J Biotechnol 135: 28–33.
21. Sakihama T, Sato T, Iwanari H, Kitamura T, Sakaguchi S, et al. (2008) A simple detection method for low-affinity membrane protein interactions by baculoviral display. PLoS ONE 3: e4024.
22. Ebihara C, Kondoh M, Hasuike N, Harada M, Mizuguchi H, et al. (2006) Preparation of a claudin-targeting molecule using a C-terminal fragment of *Clostridium perfringens* enterotoxin. J Pharmacol Exp Ther 316: 255–260.
23. Fujita K, Katahira J, Horiguchi Y, Sonoda N, Furuse M, et al. (2000) *Clostridium perfringens* enterotoxin binds to the second extracellular loop of claudin-3, a tight junction integral membrane protein. FEBS Lett 476: 258–261.
24. Takahashi A, Komiya E, Kakutani H, Yoshida T, Fujii M, et al. (2008) Domain mapping of a claudin-4 modulator, the C-terminal region of C-terminal fragment of *Clostridium perfringens* enterotoxin, by site-directed mutagenesis. Biochem Pharmacol 75: 1639–1648.
25. Meunier V, Bourrie M, Berger Y, Fabre G (1995) The human intestinal epithelial cell line Caco-2; pharmacological and pharmacokinetic applications. Cell Biol Toxicol 11: 187–194.
26. Hanna PC, Mietzner TA, Schoolnik GK, McClane BA (1991) Localization of the receptor-binding region of *Clostridium perfringens* enterotoxin utilizing cloned toxin fragments and synthetic peptides. J Biol Chem 266: 11037–11043.
27. Offner S, Hekele A, Teichmann U, Weinberger S, Gross S, et al. (2005) Epithelial tight junction proteins as potential antibody targets for pancarcinoma therapy. Cancer Immunol Immunother 54: 431–445.
28. Ling J, Liao H, Clark R, Wong MS, Lo DD (2008) Structural constraints for the binding of short peptides to claudin-4 revealed by surface plasmon resonance. J Biol Chem 283: 30585–30595.
29. Suzuki M, Kato-Nakano M, Kawamoto S, Furuya A, Abe Y, et al. (2009) Therapeutic antitumor efficacy of monoclonal antibody against Claudin-4 for pancreatic and ovarian cancers. Cancer Sci 100: 1623–1630.
30. Romani C, Comper F, Bandiera E, Ravaggi A, Bignotti E, et al. (2009) Development and characterization of a human single-chain antibody fragment against claudin-3: a novel therapeutic target in ovarian and uterine carcinomas. Am J Obstet Gynecol 201: 70 e71–79.
31. Furuse M, Furuse K, Sasaki H, Tsukita S (2001) Conversion of zonulae occludentes from tight to leaky strand type by introducing claudin-2 into Madin-Darby canine kidney I cells. J Cell Biol 153: 263–272.
32. Furuse M, Sasaki H, Tsukita S (1999) Manner of interaction of heterogeneous claudin species within and between tight junction strands. J Cell Biol 147: 891–903.
33. Umeda K, Ikenouchi J, Katahira-Tayama S, Furuse K, Sasaki H, et al. (2006) ZO-1 and ZO-2 independently determine where claudins are polymerized in tight-junction strand formation. Cell 126: 741–754.
34. Masuda K, Itoh H, Sakihama T, Akiyama C, Takahashi K, et al. (2003) A combinatorial G protein-coupled receptor reconstitution system on budded baculovirus. J Biol Chem 278: 24552–24562.
35. Hayashi I, Urano Y, Fukuda R, Isoo N, Kodama T, et al. (2004) Selective reconstitution and recovery of functional gamma-secretase complex on budded baculovirus particles. J Biol Chem 279: 38040–38046.
36. Saeki R, Kondoh M, Kakutani H, Tsunoda S, Mochizuki Y, et al. (2009) A novel tumor-targeted therapy using a claudin-4-targeting molecule. Mol Pharmacol 76: 918–926.

Biomaterials 32 (2011) 5498–5504

Contents lists available at ScienceDirect

Biomaterials

journal homepage: www.elsevier.com/locate/biomaterials

Fine tuning of receptor-selectivity for tumor necrosis factor-α using a phage display system with one-step competitive panning

Yasuhiro Abe [a], Tomoaki Yoshikawa [a,b], Masaki Inoue [a], Tetsuya Nomura [a], Takeshi Furuya [a,b], Takuya Yamashita [a,b], Kazuya Nagano [a], Hiromi Nabeshi [a,b], Yasuo Yoshioka [a,c], Yohei Mukai [a,b], Shinsaku Nakagawa [b,c], Haruhiko Kamada [a,c], Yasuo Tsutsumi [a,b,c], Shin-ichi Tsunoda [a,b,c,*]

[a] Laboratory of Biopharmaceutical Research, National Institute of Biomedical Innovation, 7-6-8 Saito-Asagi, Ibaraki, Osaka 567-0085, Japan
[b] Graduate School of Pharmaceutical Sciences, Osaka University, 1-6 Yamadaoka, Suita, Osaka 565-0871, Japan
[c] The Center of Advanced Medical Engineering and informatics, Osaka University, 1-6 Yamadaoka, Suita, Osaka 565-0871, Japan

ARTICLE INFO

Article history:
Received 24 March 2011
Accepted 5 April 2011
Available online 5 May 2011

Keywords:
Cytokine
Molecular biology
Protein
Affinity
Bioactivity

ABSTRACT

Tumor necrosis factor-α (TNF) is one of the attractive targets for the development of anti-inflammatory and anti-tumor drugs, because it is an important mediator in the pathogenesis of several inflammatory diseases and tumor progression. Thus, there is an increasing need to understand the TNF receptor (TNFR1 and TNFR2) biology for the development of TNFR-selective drugs. Nonetheless, the role of TNFRs, especially that of TNFR2, remains poorly understood. Here, using a unique competitive panning, we optimized our phage display-based screening technique for isolating receptor-selective TNF mutants, and identified several TNFR2-specific TNF mutants with high TNFR2 affinity and full bioactivity via TNFR2. Among these mutants, the R2-7 clone revealed very high TNFR2-selectivity (1.8×10^5 fold higher than that for the wild-type TNF), which is so far highest among the reported TNFR2-selective TNF mutants. Because of its high TNFR2-selectivity and full bioactivity, the TNF mutant R2-7 would not only help in elucidating the functional role of TNFR2 but would also help in understanding the structure-function relationship of TNF/TNFR2. In summary, our one-step competitive panning system is a simple, useful and effective technology for isolating receptor-selective mutant proteins.

1. Introduction

Tumor necrosis factor-α (TNF) is a major inflammatory cytokine that plays a central role in host defense and inflammation via two receptor subtypes, TNF receptor (TNFR)1 and TNFR2 [1,2]. Elevated serum levels of TNF correlates with the severity and progression of the inflammatory diseases such as rheumatoid arthritis (RA), inflammatory bowel disease, septic shock, multiple sclerosis and hepatitis [3–5]. Currently, TNF-neutralization therapies have proven successful for the treatment of RA [4,6,7]. However, these therapies can cause serious side effects, such as tuberculosis, because TNF-dependent host defense functions are also inhibited [8,9]. Therefore, understanding the function of TNF/TNFRs is important for optimal therapy of various TNF-related autoimmune diseases. TNFR1 is constitutively expressed in most tissues and seems to be the key mediator of TNF signaling [10,11]. In contrast, the expression of TNFR2 is more restricted and is found mainly on certain T-cell subpopulations [12], endothelial cells, cardiac myocytes [13] and neuronal tissue [14,15]. Recent studies suggested that TNFR2 signaling is associated with T-cell survival [16], cardioprotection [17,18], remyelination [19], and survival of some neuron subtypes [20,21]. Although the two TNFRs have been shown to have distinct functions in some cells [22], the physiological significance of the presence of both receptors is not fully understood. Especially TNFR2-induced signaling remains elusive and need further investigation.

In order to understand the mechanism of TNFRs, we have investigated the relationship between the biological activities and structural properties of a large number of TNF mutants by phage-display technique [23,24]. However, screening efficiency of isolating TNFR2-selective TNF mutants using this technique is extremely low, and it is difficult to prepare large repertoire of TNFR2-selective TNF mutants for the structure-activity relationship study. In our previous study, we screened 500 phage clones

* Corresponding author. Laboratory of Biopharmaceutical Research, National Institute of Biomedical Innovation, 7-6-8 Saito-Asagi, Ibaraki, Osaka 567-0085, Japan. Tel.: +81 72 641 9814; fax: +81 72 6419817.
E-mail address: tsunoda@nibio.go.jp (S.-i. Tsunoda).

0142-9612/$ – see front matter © 2011 Elsevier Ltd. All rights reserved.
doi:10.1016/j.biomaterials.2011.04.018

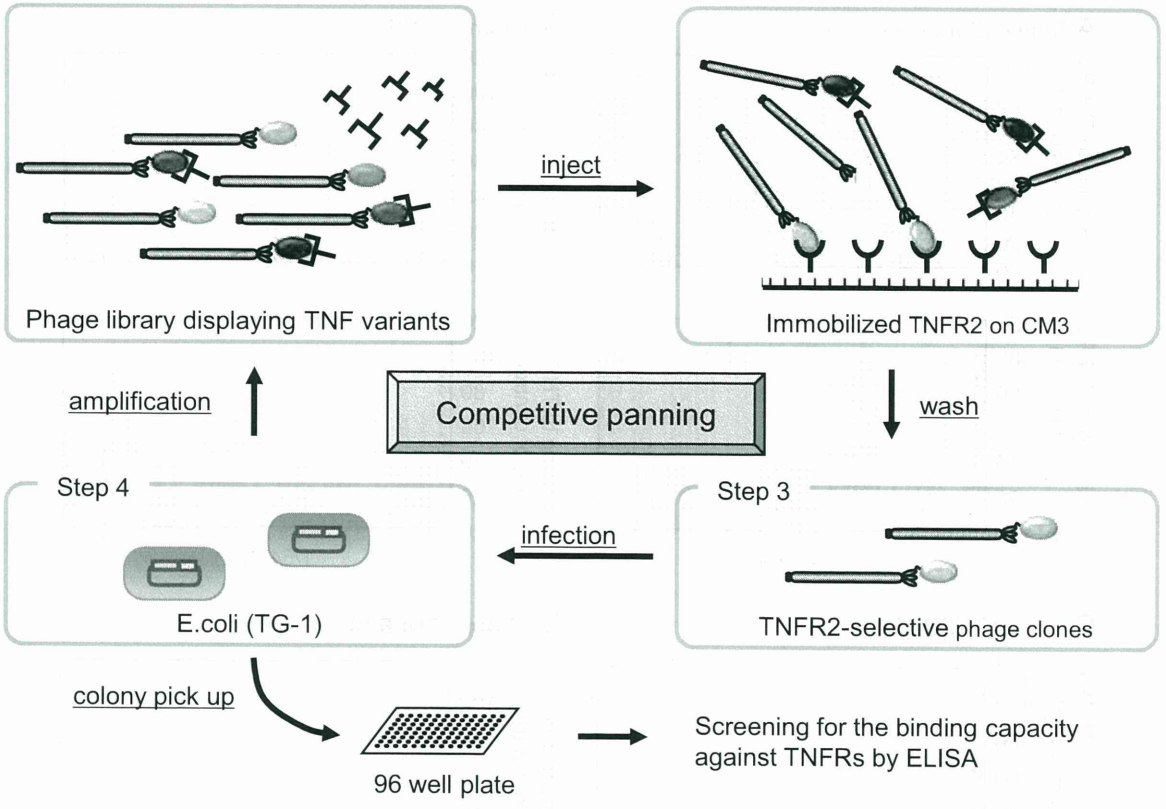

Fig. 1. Screening scheme for isolating TNFR2-selective TNF mutants using competitive panning. To concentrate TNFR2-selective mutant TNFs, phage libraries were pre-incubated with TNFR1 Fc chimera (TNFR1-Fc), and subsequent biopanning against the TNFR2 was carried out in the presence of TNFR1-Fc using the BIAcore biosensor. After several rounds of panning, phage clones were isolated and screened by ELISA.

for isolating TNFR2-selective mutants using the conventional panning method [23]. Out of the 500 clones, only 2 clones showed selectivity for TNFR2 binding that was 10-times higher than the wild-type TNF (wtTNF). Furthermore, bioactivities of these two TNFR2 selective TNF mutants were lower than that of wtTNF (<30%). To improve the screening efficacy, we optimized our phage display-based cytokine mutagenesis technology [25] with an unique competitive panning technique for identifying TNFR2-specific TNF mutants with higher affinity and bioactivity. In this competitive panning technique, phage libraries were pre-incubated with TNFR1 Fc chimera (TNFR1-Fc), and subsequent biopanning against the TNFR2 was carried out in the presence of TNFR1-Fc using the BIAcore biosensor. Since TNFR1-binding clones could not bind to TNFR2 due to steric hindrance, TNF mutants binding only to TNFR2 were selectively enriched with high efficiency. Using this optimized competitive panning technique, we have identified TNFR2-selective TNF mutants with full bioactivity via TNFR2.

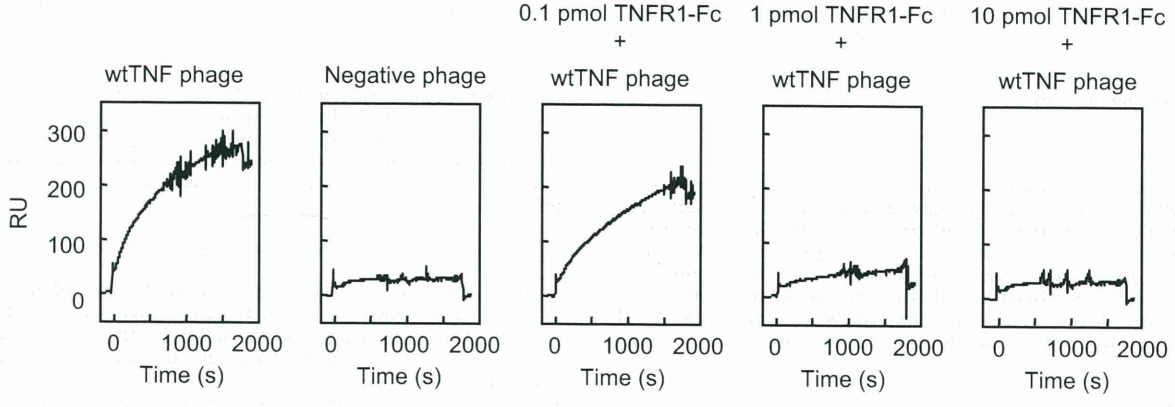

Fig. 2. Optimization of competitive panning using BIAcore biosensor. 0.1 pmol, 1 pmol or 10 pmol of human TNFR1-Fc was mixed with 1×10^{10} CFU phages displaying wtTNF for 2 h at 4 °C, and the mixture was passed over the TNFR2-immobilized CM3 sensor chip and real-time biomolecular interaction analyses were performed with BIAcore biosensor. Anti-CD25 single chain Fv-displaying phage was used as a negative control.

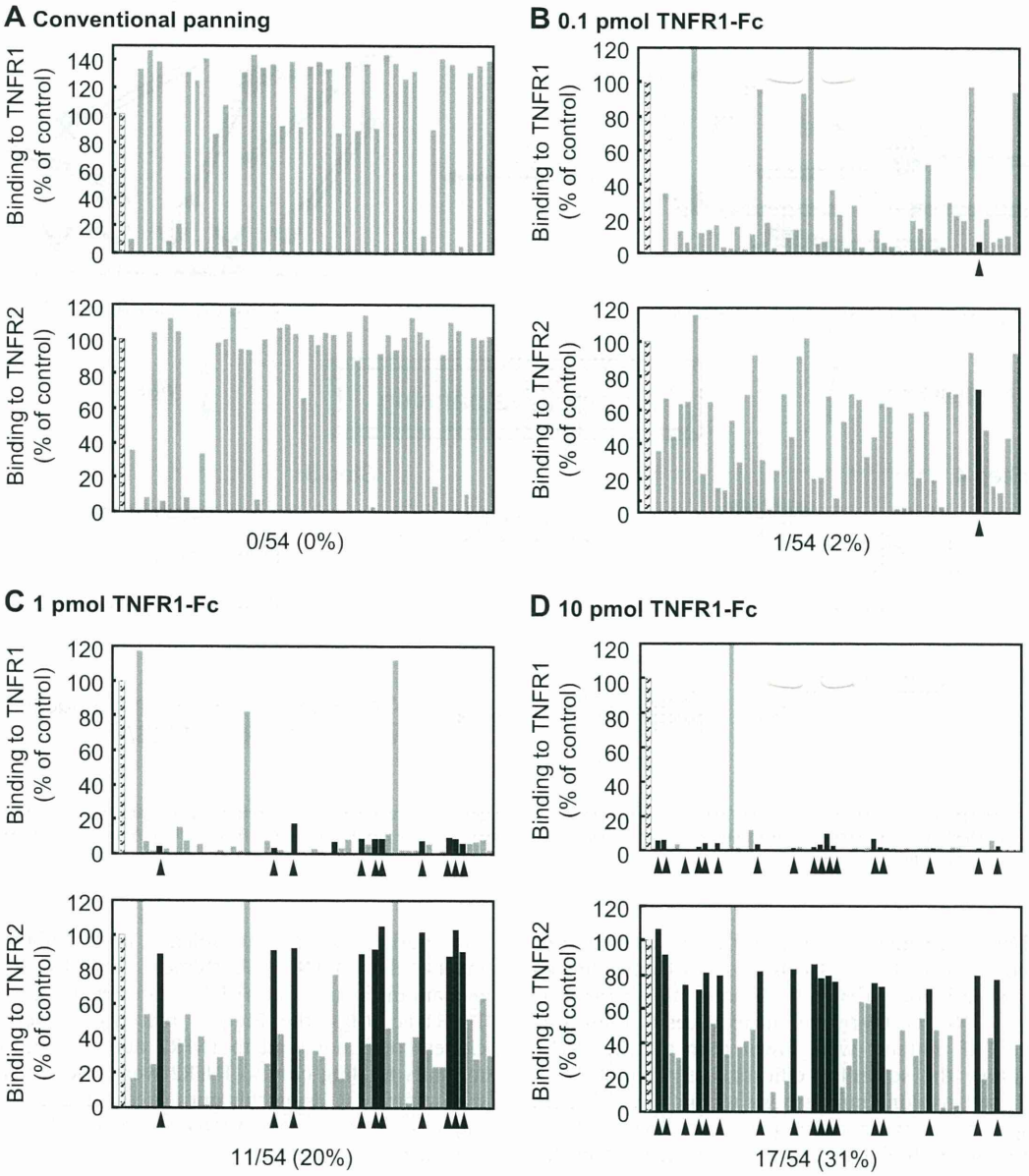

Fig. 3. Determination of relative affinities of mutant TNFs for TNFR1 or TNFR2 by capture ELISA. *E. coli* supernatant containing a TNF mutant (gray bar) from each panning conditions, in which phages were premixed with (A) none, (B) 0.1 pmol, (C) 1 pmol and (D) 10 pmol of TNFR1-Fc, were applied to the TNFR1-Fc or TNFR2-Fc immobilized plate and detected with biotinylated polyclonal anti-TNF antibody. wtTNF was used as a positive control (hatched bar). Affinities of TNFR2-selective clones (black bar) for TNFR2 was more than 70% of that of the wtTNF, and that for TNFR1 was less than 30% of that of the wtTNF.

2. Materials and methods

2.1. Cells

HEp-2 cells, a human fibroblast cell line, were provided by Cell Resource Center for Biomedical Research (Tohoku University, Sendai, Japan) and were maintained in RPMI 1640 (Sigma–Aldrich Japan, Tokyo, Japan) supplemented with 10% bovine fetal serum (FBS) 1 mM sodium pyruvate, 50 mM 2-mercaptoethanol, and antibiotics. hTNFR2/mFas-PA cells are preadipocytes derived from TNFR1$^{-/-}$R2$^{-/-}$ mice expressing a chimeric receptor, the extracellular and transmembrane domain of human TNFR2, and intracellular domain of mouse Fas; these cells were cultured in RPMI 1640 supplemented with 10% FBS, 5 μg/ml Blasticidin S HCl (Invitrogen, Carlsbad, CA), and antibiotics [26].

2.2. Library construction

Protocol for the construction of phage-display library displaying structural mutants of human TNF has been described previously [23]. In brief, multiple-mutations were introduced into the wtTNF gene by PCR to randomly replace the codons of 6 amino acid residues at positions 29, 31, 32, 145, 146 and 147, respectively, of the TNF protein. The PCR product was digested with the restriction enzymes Hind III and Not I, and ligated into the Hind III/Not I digested pY03′ phagemid vector for displaying the TNF mutants on the phage surface as g3p-fusion proteins.

2.3. Optimization of competitive panning using BIAcore biosensor

Human TNFR2-Fc (R&D systems, Minneapolis, MN) was diluted to 50 μg/ml in 10 mM sodium acetate buffer (pH 4.5) and immobilized onto a CM3 sensor chip using an amine coupling kit (GE Healthcare, UK), which resulted in an increase of 5000–6000 resonance units (RU). 0.1 pmol, 1 pmol or 10 pmol of human TNFR1-Fc (R&D systems) was mixed with 100 μl of wtTNF-displaying phage (1×10^{11} CFU/ml) for 2 h at 4 °C, and the mixture was passed over the TNFR2-immobilized CM3 sensor chip at a flow rate of 3 μl/min. The binding kinetics of the mixtures to TNFR2-Fc were analyzed by BIAcore 2000 (GE Healthcare).

Table 1
Amino acid sequences of wtTNF and TNFR2-selective TNF mutants.

Clone	Residue position					
	29	31	32	145	146	147
wtTNF	L	R	R	A	E	S
R2–6	L	R	R	H	E	D
R2–7	V	R	R	D	D	D
R2–8	L	R	R	N	D	D
R2–9	L	R	R	T	S	D
R2–10	L	R	R	Q	D	D
R2–11	L	R	R	T	D	D
R2–12	L	R	R	D	G	D
R2–13	L	R	R	D	E	D

2.4. Selection of phage displaying TNFR2-selective TNF mutants by competitive panning

1×10^{10} CFU phages displaying TNF mutants were pre-incubated for 2 h at 4 °C, with serially diluted TNFR1-Fc. The mixtures were injected at 3 μl/min over the sensor chip. After injection, the sensor chip was washed using the rinse command for 3 min. Elution was carried out using 20 μl of 10 mM glycine-HCl (pH 2.0) and the eluted phage was neutralized with 1 M Tris–HCl (pH 6.9). The recovered phages were amplified by infection of E. coli strain TG1 (Stratagene, La Jolla, CA), which allow read-through of the amber stop codon located between the TNF and g3p sequences of pY03′ phagemid vector. These steps were repeated twice. After final round of panning, the phage mixture was used to infect E. coli and plated on LB agar/ampicillin plates. Single clones of transfected TG1 were randomly picked from the plate and each colony was grown in 2-YT medium with ampicillin (100 μg/ml) and glucose (2% w/v) at 37 °C until the OD_{600} of the culture medium reached 0.4. Each culture was centrifuged, the supernatants were removed, and fresh 2-YT media with ampicillin (100 μg/ml) was added to each E. coli pellet. After incubation for 6 h at 37 °C supernatants were collected and used to determine affinity for TNFRs by capture ELISA as described previously [24]. After the procedure, the phagemid vectors were sequenced using a Big Dye Terminator v3.1 kit and ABI PRISM 3100 (Applied Biosystems Ltd., Pleasanton, CA).

2.5. Expression and purification of TNF mutants

Preparation of purified recombinant protein was described previously [25]. In brief, TNF mutants recombined into pYas1 vector, under the control of T7 promoter, were produced in E. coli (BL21λDE3). Mutant TNFs recovered from inclusion body, which were washed in Triton X-100 and solubilized in 6 M guanidine-HCl, 0.1 M Tris–HCl, pH 8.0, and 2 mM EDTA. Solubilized protein was adjusted to 10 mg/ml and was reduced with 10 mg/ml dithioerythritol for 4 h at RT and refolded by 100-fold dilution in a refolding buffer (100 mM Tris–HCl, 2 mM EDTA, 1 M arginine, and oxidized glutathione (551 mg/L)). After dialysis with 20 mM Tris–HCl, pH 7.4, containing 100 mM urea, active trimeric proteins were purified by Q-Sepharose (GE Healthcare)chromatography and size-exclusion chromatography (Superose 12; GE Healthcare).

2.6. Analysis of binding kinetics using surface plasmon resonance (SPR)

The binding kinetics of the wtTNF and TNF mutants were analyzed by the SPR technique (BIAcore 2000; GE Healthcare). TNFR1-Fc or TNFR2-Fc were separately immobilized on to CM5 sensor chip, resulting in an increase of 3000–3500 RU. During the association phase, wtTNF or TNF mutants diluted in running buffer (HBS-EP) at 156.8, 52.3, 17.4, 5.8 or 1.9 nM were passed over the immobilized TNFR2 for 2 min at a flow rate of 20 μl/min. During the dissociation phase, HBS-EP was run over the sensor chip for 1 min at a flow rate of 20 μl/min. The SPR measurements for TNFR1 were performed using much higher concentrations of TNF mutants (392.1, 130.7, 43.6, 14.5 or 4.8 nM). The data were analyzed globally with BIAevaluation 3.1 software (GE Healthcare) to apply a 1:1 Langmuir binding model. The obtained sensorgrams were fitted globally over the range of injected concentrations and simultaneously over the association and dissociation phages.

2.7. In vitro assessment of bioactivity via TNFR1 or TNFR2 with TNF mutants

HEp-2 cells were seeded at 4×10^4 cells/well in 96-well plates and incubated for 18 h with serially diluted wtTNF (Peprotech, Rocky Hill, NJ) or TNF mutants in the presence of 50 mg/ml cycloheximide. After incubation, cell survival was determined by methylene blue assay as described previously [25]. In the case of analyzing TNFR2-mediated biological activity, hTNFR2/mFas-PA were seeded on 96-well micro titer plates with a density of 1.5×10^4 cells/well in culture medium. Serial dilutions of wtTNF (Peprotech) and TNF mutants were prepared with 1 μg/ml cycloheximide and added to each well. After 48 h-incubation at 37 °C, the cell viabilities were analyzed using a WST-8 assay kit (Nacalai Tesque) according to the manufacturer's instructions.

3. Results

3.1. Optimization of one-step competitive panning protocol

To improve identifying TNFR2-selective TNF mutants with better bioactivity, we have introduced a step to remove the TNFR1-binding phages from the library by competitive panning using TNFR1-Fc. We postulated that TNFR1-binding clones could be eliminated when panning for the TNFR2-binding clones is performed in the presence of TNFR1 protein (see Fig. 1). Although an immunoplate or immunotube is commonly used for the panning [27–29], these techniques cannot make real-time observation of the interaction between phage library and receptor, and are difficult to automate and control the precise settings. Therefore, we first utilized the BIAcore biosensor and optimized the concentration of TNFR1-Fc required for eliminating the TNFR1-binding clones. Serially diluted human TNFR1-Fc was mixed with 1×10^{10} CFU phages displaying wtTNF, and the binding avidity of the phage-displayed wtTNF for TNFR2 was assessed using a BIAcore biosensor. As shown in Fig. 2, TNFR1-Fc inhibited the binding of phage-displayed wtTNF to TNFR2 in a dose-dependent manner. 10 pmol of TNFR1-Fc virtually abolished the binding of wtTNF not only to TNFR2 (last panel in Fig. 2) but also the binding of wtTNF to TNFR1 (data not shown). These results clearly suggest that 10 pmol of TNFR1-Fc would be sufficient for competitively subtract unwanted TNFR1-binding phage clones from a phage library displaying structural TNF mutants.

Table 2
Biding kinetics of TNFs to TNFR1 and TNFR2.

	TNFR1				TNFR2			
	k_{on}[a] (10^6 $M^{-1}s^{-1}$)	k_{off}[b] (10^{-4} s^{-1})	K_D[c] (10^{-10} M)	Relative[d] (%)	k_{on}[a] (10^6 $M^{-1}s^{-1}$)	k_{off}[b] (10^{-4} s^{-1})	K_D[c] (10^{-10} M)	Relative[d] (%)
wtTNF	0.45	1.3	2.9	100.0	2.0	12.1	6.1	100.0
R2–6	0.79	54.5	68.8	4.2	3.2	7.8	2.4	251.4
R2–7	0.44	116.0	262.0	1.1	2.1	7.4	3.6	169.7
R2–8	1.22	50.3	41.1	7.1	3.1	6.6	2.1	291.0
R2–9	1.19	50.1	42.3	6.9	3.8	12.6	3.3	185.2
R2–10	0.67	43.9	63.7	4.6	2.2	5.3	2.4	253.5
R2–11	0.81	87.5	108.	2.7	2.3	5.4	2.3	264.5
R2–12	1.36	98.8	72.6	4.0	4.1	10.6	2.6	235.0
R2–13	0.97	104.0	107.0	2.7	2.9	8.2	2.9	212.2

Kinetic parameters for each TNF were calculated from the respective sensorgram by BIAevaluation 3.1software, and taking into consideration that the TNF binds as a trimer.
[a] k_{on} is the association kinetic constant.
[b] k_{off} is the dissociation kinetic constant.
[c] K_D is the equilibrium dissociation constant ($K_D = k_{off}/k_{on}$).
[d] Relative values were calculated from the K_D (wtTNF)/K_D (TNF mutants) × 100.

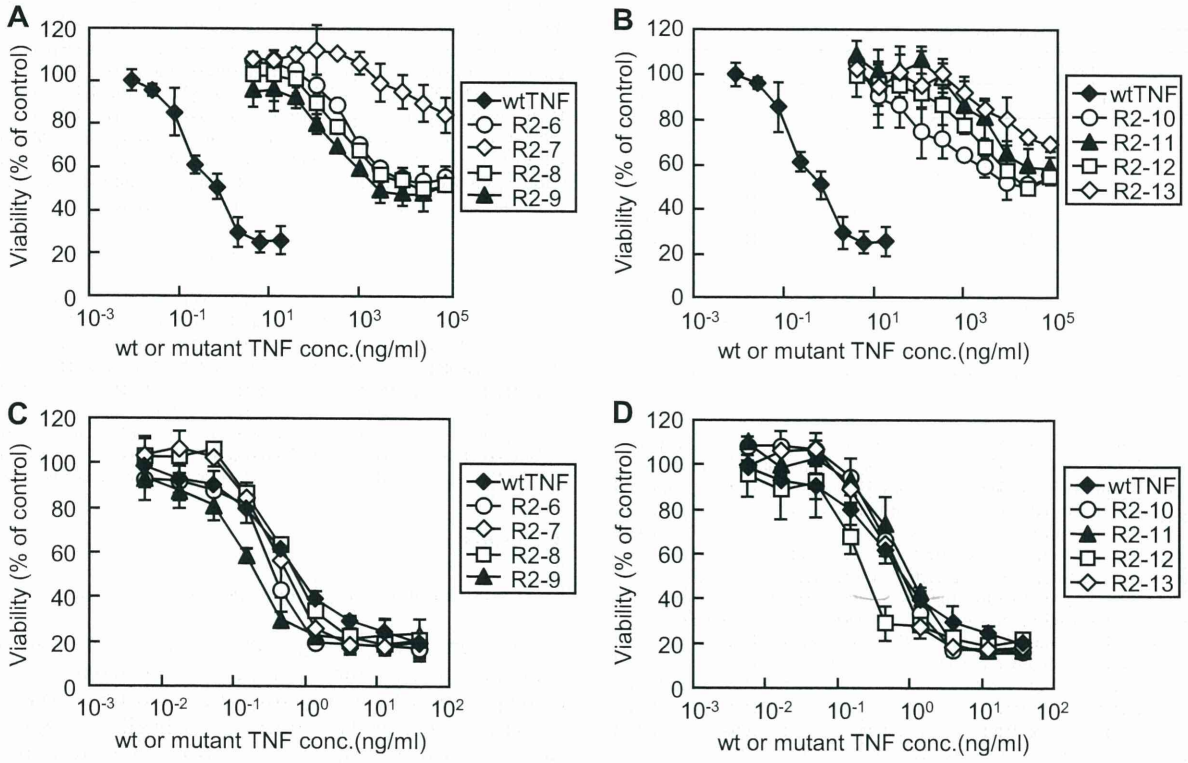

Fig. 4. In vitro bioactivity assay of TNF mutants via TNFR1 or TNFR2. The bioactivity of mutant TNFs via TNFR1 or TNFR2 were measured by cytotoxicity assay against HEp-2 cells (A and B) or hTNFR2/mFas-PA (C and D), respectively. Each point represents the mean ± S.D. of triplicate measurements.

3.2. Selection of TNFR2-selective TNF mutants by one-step competitive panning

To concentrate TNFR2-selective mutant TNFs, the TNF structural mutant displaying phage library was subjected to two rounds of conventional panning or competitive panning against TNFR2 using the BIAcore biosensor. After the second round of panning, *Escherichia coli* (TG1) supernatants of 54 randomly picked clones from each panning procedure were further screened by capture ELISA to analyze their binding specificities for each TNFR (Fig. 3). Consequently, we obtained numerous clones with high-affinity for TNFR2 under all panning conditions. Binding avidities of these clones for TNFR1 tended to decrease depending on the concentration of TNFR1-Fc used for premixing. However, binding avidity of a TNFR2-selective clone, which binds only to TNFR2 (Fig. 3, black bar), tended to increase depending on the concentration of TNFR1-Fc used for premixing. Almost all clones obtained from the conventional and competitive panning with 0.1 pmol of TNFR1-Fc (Fig. 3A and B, respectively) bound to TNFR1, and the panning efficiency for isolating the TNFR2-selective TNF mutants was <2%. In contrast, clones obtained from the subtracted panning with 1 or 10 pmol of TNFR1-Fc (Fig. 3C and D, respectively) contained many TNFR2-selective TNF mutants (>20%). From these panned clones, we eventually identified eight candidate agonists that selectively and strongly bound to the TNFR2. Amino acid sequences of these eight candidate TNFR2-selective TNF mutants are shown in Table 1. TNFR2-slective mutants were mutated near residue 145 and

Table 3
In vitro bioactivities of TNF mutants via TNFR1 or TNFR2.

	TNFR1[a]		TNFR2[b]		TNFR2/TNFR1[e]
	EC50[c] (ng/ml)	Relative Activity[d] (%)	EC50[c] (ng/ml)	Relative activity[d] (%)	
wtTNF	0.6	100	0.56	100	1.0
R2–6	8.1×10^{3}	7.3×10^{-3}	0.39	144	2.0×10^{4}
R2–7	$>1.0 \times 10^{5}$	$<6.0 \times 10^{-4}$	0.51	110	1.8×10^{5}
R2–8	4.6×10^{3}	1.2×10^{-2}	0.67	84	7.0×10^{3}
R2–9	2.1×10^{3}	2.8×10^{-2}	0.21	267	9.5×10^{3}
R2–10	1.1×10^{4}	5.4×10^{-3}	0.72	78	1.4×10^{4}
R2–11	6.7×10^{4}	8.9×10^{-4}	0.95	59	6.6×10^{4}
R2–12	2.6×10^{4}	2.2×10^{-3}	0.23	243	1.1×10^{5}
R2–13	$>1.0 \times 10^{5}$	$<6.0 \times 10^{-4}$	0.63	89	1.5×10^{5}

[a] Bioactivities of the wtTNF and TNF mutants via TNFR1 were measured by determining the TNF-induced cytotoxicity in HEp-2 cells.
[b] Bioactivities of the wtTNF and TNF mutants via TNFR2 were measured by determining the TNF-induced cytotoxicity in hTNFR2/mFas-PA.
[c] Experimental data were analyzed by a logistic regression model to calculate the mean effective concentration (EC50).
[d] Relative activities were calculated from the EC50 (wtTNF)/EC50 (TNF mutants).
[e] Selectivity for TNFR2 was calculated from the ratio of the relative activity (via TNFR2)/relative activity (via TNFR1).

conserved near residue 30. These findings indicate that the amino acid residues near position 30 are an essential for TNFR2 binding.

3.3. Binding kinetics of TNFR2-selective TNF mutants

To investigate the properties of eight TNFR2-selective TNF mutants in detail, we prepared recombinant protein using the previously described methods [30,31]. TNF mutants expressed as an inclusion body in *E. coli* (BL21λDE3) were denatured and refolded. Then, active TNF mutants were purified by ion–exchange and gel–filtration chromatography. TNF mutant purity was greater than 90% in sodium dodecyl sulfate–polyacrylamide gel electrophoresis, and all mutants were confirmed to form homotrimers in the same manner as the wtTNF by gel-filtration analysis (data not shown). To analyze the binding properties of these TNFR2-selective TNF mutants, we determined their binding dissociation constants (kinetic on- and off-rates) for TNFR1 and TNFR2, respectively, in detail using the surface plasmon resonance technique (Table 2). Our analysis showed that all eight mutant TNFs bound to the TNFR2 with high affinity; in contrast, they bound to the TNFR1 with greatly reduced affinity (typically between 1 and 7% of the wtTNF affinity). The dissociation constants (K_D) of these mutants for TNFR2 were between 2.1–3.6 $\times$ 10^{-10} M, and their relative affinities for TNFR2 were between 169 and 291% of that of the wtTNF. Thus, using the competitive panning technique we successfully obtained a large repertoire of TNFR2-selective TNF mutants with different binding parameters (on- and off-rates and dissociation constants).

3.4. Bioactivities of TNFR2-selective TNF mutants

To examine the bioactivity of these TNF mutants via TNFR1, we subsequently performed a cytotoxicity assay using HEp-2 cells (Fig. 4A and B). All TNF mutants (R2-6 ~ R2-13) showed almost no cytotoxicity, and the bioactivity was much lower than that of the wtTNF. Next, we evaluated the TNFR2-mediated activity of TNF mutants using the hTNFR2/mFas-PA, which were previously constructed in our laboratory [26]. The TNFR2-mediated bioactivities of these 8 mutant TNF proteins were at least same or higher than that of the wtTNF (Fig. 4C and D). As a negative control, we determined TNF cytotoxicity in parental TNFR1$^{-/-}$R2$^{-/-}$ preadipocytes and observed no wtTNF- or mutant TNF-mediated cell death (data not shown). Results of the cytotoxicity assay are summarized in Table 3. R2-7, the most highly TNFR2-selective mutant, exhibited 1.8 $\times$ 10^5 fold higher TNFR2-selectivity than that for the wild-type TNF.

4. Discussion

Recently, it was revealed that the two TNFRs worked together by crosstalk signaling, which suggested that the TNF-mediated signaling in the presence of both TNF receptors actually correlates with their physiological functions [32–34]. To understand the mechanism as well as to analyze the structure–function relationship of the TNFRs, several attempts were made in the past to create TNFR-specific mutant TNFs by conventional site-directed mutagenesis methods (such as Kunkel's method) [35–37]. However, these attempts were not very successful in yielding a desired TNF mutant having high receptor specificity and full bioactivity. For example, the TNFR2-binding affinity of the double mutant D143N-A145R was about 5–10 fold less than the wtTNF [38]. To overcome these problems, we applied phage-display technique and optimized panning method using the BIAcore biosensor (Fig. 1). Using an adequate amount of selective competitive inhibitor (>1 pmol TNFR1-Fc), this one-step competitive panning is ten times more efficient for screening TNFR2-selective TNF mutants, suggesting the competitive panning technology described here is a simple and effective screening method for fine-tuning TNF receptor-selectivity (Fig. 3). As a result of screening, we obtained successfully obtained TNFR2-selective TNF mutants with full bioactivity via TNFR2 (Table 3). Because of its high TNFR2-selectivity and full bioactivity, the TNF mutant R2-7 would help in elucidating the functional role of TNFR2.

One advantage of our phage-display-based technique is that it can be used to obtain the sequence information of many mutants [39,40]. It was previously shown by site-specific mutagenesis technique that mutations at positions 29, 31 and 32 (L29S, R31E and R32W) remarkably reduced the TNF's affinity for binding to TNFR2 [35,37,38]. For most of the TNFR2-selective TNF mutants, amino acids at positions 29, 31 and 32 were indeed identical (except for the R2-7 mutant which contained a conserved L to V substitution at position 29) to those of the wtTNF (Table 1), which is consistent with the previously reported idea that these three amino acids play critical roles in maintaining the binding between the TNF and TNFR2. The amino acid sequence at positions 145, 146 and 147 of the TNFR2-selective TNF mutants were, however, very different from those of the wtTNF. For example, the amino acid residue at position 145 of the TNF mutants R2-7, R2-12 and R2-13 contained an Asp residue in place of the Ala residue, and all of them showed high TNFR2 selectivity. Structural analysis and mutagenesis studies suggested that the loop containing the residues 145–147 is involved in the receptor binding [41–43]. Since Asp is a comparatively large residue, we speculated that this substitution could lead to a steric hindrance disrupting the interaction between the TNFR1 and TNFR2-selective mutants, which may be why they are less TNFR1-selective. However, why this replacement would increase the selectivity for TNFR2 is unclear at this moment. Currently, we are working on determining the structure of the TNF/TNFR2 complex by X-ray crystallography [44] so that structure–activity relationship studies could be initiated in the near future. Additionally, this structural information, in combination with bioinformatics technology, will be useful for designing TNFR-selective inhibitors (peptide mimics and chemical compounds).

5. Conclusions

In this study, we optimized our phage display-based screening using a unique competitive panning technique, which is ten times more efficient for screening TNFR2-selective TNF mutants compared to the conventional panning method. As a result of screening, we have succeeded in isolating several TNFR2-specific TNF mutants with high TNFR2 affinity and full bioactivity via TNFR2. Further analysis of the relationship between the structure and bioactivity of the TNF mutants would offer highly valuable and useful information regarding the TNF/TNFR biology. In conclusion, our fine-tuned competitive panning system is a simple and effective technology for isolating receptor-selective mutant proteins.

Acknowledgment

This study was supported in part by Grants-in-Aid for Scientific Research from the Ministry of Education, Culture, Sports, Science and Technology of Japan, and from the Japan Society for the Promotion of Science (JSPS). This study was also supported in part by Health Labour Sciences Research Grants from the Ministry of Health, Labor and Welfare of Japan, and by Health Sciences Research Grants for Research on Publicly Essential Drugs and Medical Devices from the Japan Health Sciences Foundation.

References

[1] Aggarwal BB. Signalling pathways of the TNF superfamily: a double-edged sword. Nat Rev Immunol 2003;3(9):745–56.
[2] Szlosarek PW, Balkwill FR. Tumour necrosis factor alpha: a potential target for the therapy of solid tumours. Lancet Oncol 2003;4(9):565–73.

[3] Aderka D, Engelmann H, Maor Y, Brakebusch C, Wallach D. Stabilization of the bioactivity of tumor necrosis factor by its soluble receptors. J Exp Med 1992; 175(2):323–9.
[4] Feldmann M, Maini RN. Lasker Clinical Medical Research Award. TNF defined as a therapeutic target for rheumatoid arthritis and other autoimmune diseases. Nat Med 2003;9(10):1245–50.
[5] Muto Y, Nouri-Aria KT, Meager A, Alexander GJ, Eddleston AL, Williams R. Enhanced tumour necrosis factor and interleukin-1 in fulminant hepatic failure. Lancet 1988;2(8602):72–4.
[6] Thorbecke GJ, Shah R, Leu CH, Kuruvilla AP, Hardison AM, Palladino MA. Involvement of endogenous tumor necrosis factor alpha and transforming growth factor beta during induction of collagen type II arthritis in mice. Proc Natl Acad Sci U S A 1992;89(16):7375–9.
[7] Williams RO, Feldmann M, Maini RN. Anti-tumor necrosis factor ameliorates joint disease in murine collagen-induced arthritis. Proc Natl Acad Sci U S A 1992;89(20):9784–8.
[8] Gomez-Reino JJ, Carmona L, Valverde VR, Mola EM, Montero MD. Treatment of rheumatoid arthritis with tumor necrosis factor inhibitors may predispose to significant increase in tuberculosis risk: a multicenter active-surveillance report. Arthritis Rheum 2003;48(8):2122–7.
[9] Lubel JS, Testro AG, Angus PW. Hepatitis B virus reactivation following immunosuppressive therapy: guidelines for prevention and management. Intern Med J 2007;37(10):705–12.
[10] Leist M, Gantner F, Jilg S, Wendel A. Activation of the 55 kDa TNF receptor is necessary and sufficient for TNF-induced liver failure, hepatocyte apoptosis, and nitrite release. J Immunol 1995;154(3):1307–16.
[11] Mori L, Iselin S, De Libero G, Lesslauer W. Attenuation of collagen-induced arthritis in 55-kDa TNF receptor type 1 (TNFR1)-IgG1-treated and TNFR1-deficient mice. J Immunol 1996;157(7):3178–82.
[12] Ware CF, Crowe PD, Vanarsdale TL, Andrews JL, Grayson MH, Jerzy R, et al. Tumor necrosis factor (TNF) receptor expression in T lymphocytes. Differential regulation of the type I TNF receptor during activation of resting and effector T cells. J Immunol 1991;147(12):4229–38.
[13] Irwin MW, Mak S, Mann DL, Qu R, Penninger JM, Yan A, et al. Tissue expression and immunolocalization of tumor necrosis factor-alpha in post-infarction dysfunctional myocardium. Circulation 1999;99(11):1492–8.
[14] Dopp JM, Sarafian TA, Spinella FM, Kahn MA, Shau H, de Vellis J. Expression of the p75 TNF receptor is linked to TNF-induced NFkappaB translocation and oxyradical neutralization in glial cells. Neurochem Res 2002;27(11):1535–42.
[15] Yang L, Lindholm K, Konishi Y, Li R, Shen Y. Target depletion of distinct tumor necrosis factor receptor subtypes reveals hippocampal neuron death and survival through different signal transduction pathways. J Neurosci 2002; 22(8):3025–32.
[16] Ban L, Zhang J, Wang L, Kuhtreiber W, Burger D, Faustman DL. Selective death of autoreactive T cells in human diabetes by TNF or TNF receptor 2 agonism. Proc Natl Acad Sci U S A 2008;105(36):13644–9.
[17] Monden Y, Kubota T, Inoue T, Tsutsumi T, Kawano S, Ide T, et al. Tumor necrosis factor-alpha is toxic via receptor 1 and protective via receptor 2 in a murine model of myocardial infarction. Am J Physiol Heart Circ Physiol 2007;293(1):H743–53.
[18] Wang M, Crisostomo PR, Markel TA, Wang Y, Meldrum DR. Mechanisms of sex differences in TNFR2-mediated cardioprotection. Circulation 2008;118(Suppl. 14):S38–45.
[19] Arnett HA, Mason J, Marino M, Suzuki K, Matsushima GK, Ting JP. TNF alpha promotes proliferation of oligodendrocyte progenitors and remyelination. Nat Neurosci 2001;4(11):1116–22.
[20] Faustman D, Davis M. TNF receptor 2 p.thway: drug target for autoimmune diseases. Nat Rev Drug Discov 2010;9(6):482–93.
[21] Fontaine V, Mohand-Said S, Hanoteau N, Fuchs C, Pfizenmaier K, Eisel U. Neurodegenerative and neuroprotective effects of tumor Necrosis factor (TNF) in retinal ischemia: opposite roles of TNF receptor 1 and TNF receptor 2. J Neurosci 2002;22(7). RC216.
[22] MacEwan DJ. TNF receptor subtype signalling: differences and cellular consequences. Cell Signal 2002;14(6):477–92.
[23] Mukai Y, Shibata H, Nakamura T, Yoshioka Y, Abe Y, Nomura T, et al. Structure-function relationship of tumor necrosis factor (TNF) and its receptor interaction based on 3D structural analysis of a fully active TNFR1-selective TNF mutant. J Mol Biol 2009;385(4):1221–9.
[24] Shibata H, Yoshioka Y, Ohkawa A, Minowa K, Mukai Y, Abe Y, et al. Creation and X-ray structure analysis of the tumor necrosis factor receptor-1-selective mutant of a tumor necrosis factor-alpha antagonist. J Biol Chem 2008;283(2):998–1007.
[25] Yamamoto Y, Tsutsumi Y, Yoshioka Y, Nishibata T, Kobayashi K, Okamoto T, et al. Site-specific PEGylation of a lysine-deficient TNF-alpha with full bioactivity. Nat Biotechnol 2003;21(5):546–52.
[26] Abe Y, Yoshikawa T, Kamada H, Shibata H, Nomura T, Minowa K, et al. Simple and highly sensitive assay system for TNFR2-mediated soluble- and transmembrane-TNF activity. J Immunol Methods 2008;335(1–2):71–8.
[27] Schwarz M, Rottgen P, Takada Y, Le Gall F, Knackmuss S, Bassler N, et al. Single-chain antibodies for the conformation-specific blockade of activated platelet integrin alphaIIbbeta3 designed by subtractive selection from naive human phage libraries. Faseb J 2004;18(14):1704–6.
[28] Popkov M, Rader C, Barbas 3rd CF. Isolation of human prostate cancer cell reactive antibodies using phage display technology. J Immunol Methods 2004; 291(1–2):137–51.
[29] Eisenhardt SU, Schwarz M, Bassler N, Peter K. Subtractive single-chain antibody (scFv) phage-display: tailoring phage-display for high specificity against function-specific conformations of cell membrane molecules. Nat Protoc 2007;2(12):3063–73.
[30] Shibata H, Yoshioka Y, Abe Y, Ohkawa A, Nomura T, Minowa K, et al. The treatment of established murine collagen-induced arthritis with a TNFR1-selective antagonistic mutant TNF. Biomaterials 2009;30(34):6638–47.
[31] Shibata H, Yoshioka Y, Ikemizu S, Kobayashi K, Yamamoto Y, Mukai Y, et al. Functionalization of tumor necrosis factor-alpha using phage display technique and PEGylation improves its antitumor therapeutic window. Clin Cancer Res 2004;10(24):8293–300.
[32] Wajant H, Pfizenmaier K, Scheurich P. Tumor necrosis factor signaling. Cell Death Differ 2003;10(1):45–65.
[33] Weiss T, Grell M, Siemienski K, Muhlenbeck F, Durkop H, Pfizenmaier K, et al. TNFR80-dependent enhancement of TNFR60-induced cell death is mediated by TNFR-associated factor 2 and is specific for TNFR60. J Immunol 1998; 161(6):3136–42.
[34] Fotin-Mleczek M, Henkler F, Samel D, Reichwein M, Hausser A, Parmryd I, et al. Apoptotic crosstalk of TNF receptors: TNF-R2-induces depletion of TRAF2 and IAP proteins and accelerates TNF-R1-dependent activation of caspase-8. J Cell Sci 2002;115(Pt. 13):2757–70.
[35] Yamagishi J, Kawashima H, Matsuo N, Ohue M, Yamayoshi M, Fukui T, et al. Mutational analysis of structure–activity relationships in human tumor necrosis factor-alpha. Protein Eng 1990;3(8):713–9.
[36] Barbara JA, Smith WB, Gamble JR, Van Ostade X, Vandenabeele P, Tavernier J, et al. Dissociation of TNF-alpha cytotoxic and proinflammatory activities by p55 receptor- and p75 receptor-selective TNF-alpha mutants. Embo J 1994; 13(4):843–50.
[37] Van Ostade X, Vandenabeele P, Everaerdt B, Loetscher H, Gentz R, Brockhaus M, et al. Human TNF mutants with selective activity on the p55 receptor. Nature 1993;361(6409):266–9.
[38] Loetscher H, Stueber D, Banner D, Mackay F, Lesslauer W. Human tumor necrosis factor alpha (TNF alpha) mutants with exclusive specificity for the 55-kDa or 75-kDa TNF receptors. J Biol Chem 1993;268(35):26350–7.
[39] Abe Y, Nomura T, Yoshioka Y, Kamada H, Tsunoda S, Tsutsumi Y. Anti-inflammatory effects of a Novel TNFR1-selective antagonistic TNF mutant on established murine collagen-induced arthritis. Adv Exp Med Biol 2011;691:493–500.
[40] Yoshioka Y, Watanabe H, Morishige T, Yao X, Ikemizu S, Nagao C, et al. Creation of lysine-deficient mutant lymphotoxin-alpha with receptor selectivity by using a phage display system. Biomaterials 2010;31(7):1935–43.
[41] Eck MJ, Sprang SR. The structure of tumor necrosis factor-alpha at 2.6 A resolution. Implications for receptor binding. J Biol Chem 1989;264(29):17595–605.
[42] Van Ostade X, Tavernier J, Fiers W. Structure–activity studies of human tumour necrosis factors. Protein Eng 1994;7(1):5–22.
[43] Idriss HT, Naismith JH. TNF alpha and the TNF receptor superfamily: structure-function relationship(s). Microsc Res Tech 2000;50(3):184–95.
[44] Mukai Y, Nakamura T, Yoshikawa M, Yoshioka Y, Tsunoda S, Nakagawa S, et al. Solution of the structure of the TNF-TNFR2 complex. Sci Signal 2010;3(148). ra83.

Laboratory of Bio-Functional Molecular Chemistry[1], Laboratory of Toxicology and Safety Science[2], Graduate School of Pharmaceutical Sciences[3], Osaka University, Suita; Laboratory of Biopharmaceutical Research (Pharmaceutical Proteomics), National Institute of Biomedical Innovation, Ibaraki, Osaka, Japan

Effect of surface charge on nano-sized silica particles-induced liver injury

K. ISODA[1], T. HASEZAKI[1], M. KONDOH[1], Y. TSUTSUMI[2,3], K. YAGI[1]

Received October 5, 2010, accepted November 11, 2010

Dr Kiyohito Yagi, Laboratory of Bio-Functional Molecular Chemistry, Graduate School of Pharmaceutical Sciences, Osaka University, Suita, Osaka 565-0871, Japan
yagi@phs.osaka-u.ac.jp

Pharmazie 66: 278–281 (2011) *doi: 10.1691/ph.2011.0808*

Nanomaterials are used frequently in microelectronics, cosmetics and sunscreen, and research for the development of nanomaterial-based drug delivery systems is promising. We previously reported that the intravenous administration of unmodified silica particles with a diameter of 70 nm (SP70) caused hepatic injury. Here, we examined the acute hepatic toxicity of SP70 modified with amino group (SP70-N) or carboxyl group (SP70-C). When administered intravenously into mice, SP70-N and SP70-C dose-dependently increased the serum level of alanine aminotransferase (ALT). However, the toxicity levels of surface charge-modified silica particles were much less weaker than the level of unmodified particles. When SP70 was repeatedly administered at 40 mg/kg twice a week for 4 weeks into mice, the hydroxyproline content of the liver significantly increased. Azan staining of the liver section indicated the extensive fibrosis. To the contrary, the repeated administration of SP70-N or SP70-C at 60 mg/kg twice a week for 4 weeks into mice did not cause the hepatic fibrosis. These findings suggest that the surface charge of nanomaterials could change their toxicity.

1. Introduction

Recently, the scientific, medical, and technical applications of nanomaterials have greatly increased. Nanomaterials are frequently used in microelectronics, cosmetics and sunscreen, and their potential use in drug-delivery systems is being investigated (Dobson 2006). Nanomaterials have unique physicochemical qualities as compared to micromaterials in regard to size, surface structure, solubility, and aggregation. Thus, the reduction in particle size from the micro- to nanoscale is beneficial for many industrial and scientific applications. However, nanomaterials have potential toxicity that is not found in micromaterials, and it is, therefore, essential to understand the biological activity and potential toxicity of nanomaterials (Warheit et al. 2008).

The physical properties of nanomaterials are changed by the modification of their surface charge, which extends their possible applications. For example, charge-modified dendrimers are expected to have applications in drug-delivery systems. The physical properties and the toxicity of carbon nanotubes change based on the surface charge (Smith et al. 2009), as do the pharmacokinetics of liposomes. Future research will undoubtedly lead to expanded applications of surface-modified nanomaterials, however, little has been reported on their toxicity.

Silica nanoparticles have been applied to diagnostic measures and drug delivery methods. Intraperitoneal administration of silica nanoparticles results in the biodistribution of the nanoparticles to diverse organs, such as the liver, kidney, spleen and lung (Kim et al., 2006). We previously found that nano-size silica particles with a diameter of 70 nm caused liver injury, while micro-size particles with a diameter of 300 or 1000 nm did not (Nishimori et al. 2009a, b). In the present study, we examined the hepatic toxicity of surface charge-modified silica nanoparticles.

2. Investigations, results and discussion

The surface modification technology has been developed in the field of nanotechnology (Schiestel et al. 2004), and many nanomaterials with new functions will be produced for cosmetics and medicinal use. Thus, it should be important to investigate the effect of surface charge of nanomaterials on living body.

We initially examined the acute toxicity of 70-nm diameter silica nanoparticles (SP70) modified with amino group (SP70-N) or carboxyl group (SP70-C) at the maximal dose of 100 mg/kg. Intravenous injection of 50 mg/kg of unmodified SP70 was lethal in mice (Fig. 1A). The acute liver toxicity of SP70-N and SP70-C increased in a dose-dependent manner (Fig. 1B, C). Intravenous injection of SP70-C was lethal in all mice at 100 mg/kg and was often lethal at 80 and 60 mg/kg. SP70-C was more toxic than SP70-N. We examined the hepatic injury caused by 40 mg/kg of unmodified SP70 and 60 mg/kg of modified SP70 (SP70-C and SP70-N). The hematoxylin-eosin staining of liver tissue from mice injected with the silica nanoparticles is shown in Fig. 2A–D. The liver injury caused by SP70 was more extensive than that caused by SP70-C and SP70-N. Significant increase in the levels of BUN, a biochemical marker of kidney injury, was not observed in mice that received the nanoparticles (Fig. 3). The less amount of unmodified SP70 induced significant liver damage than the surface-modified silica particles. Thus, the

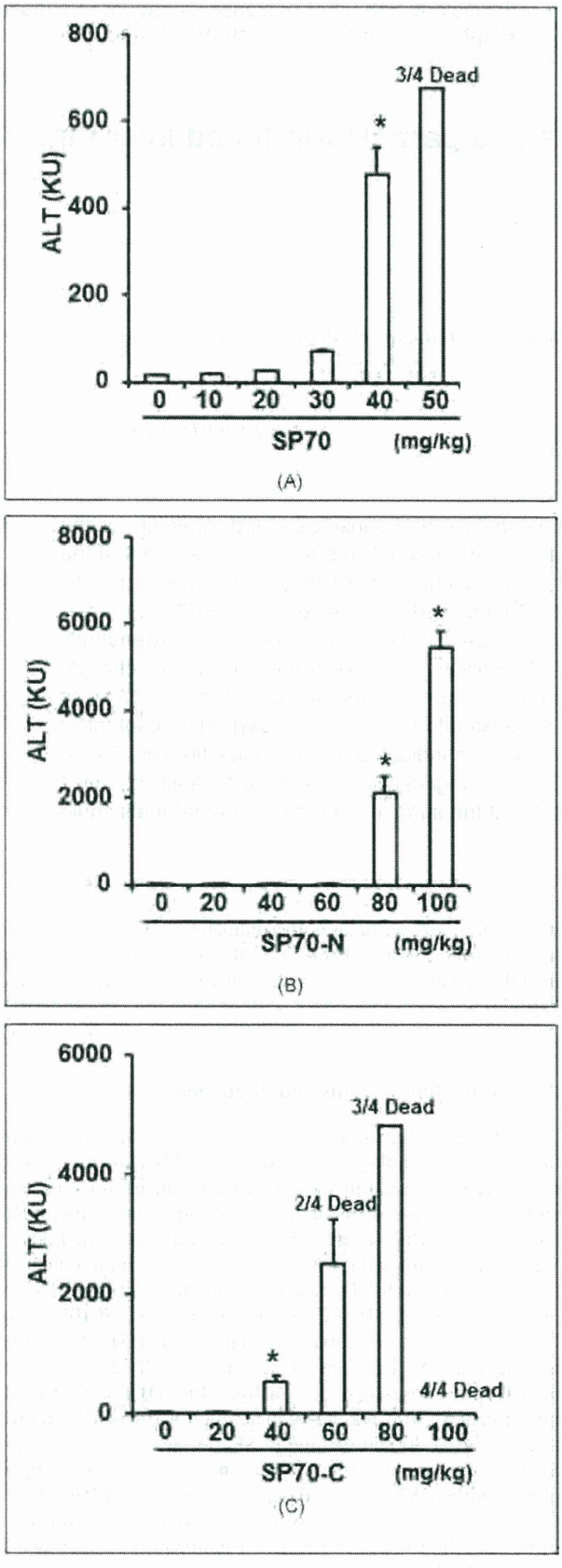

Fig. 1: Acute liver toxicity of SP70-N and SP70-C. SP70 (A), SP70-N (B) and SP70-C (C) were intravenously administered at the indicated doses. At 24 h after administration, blood was collected, and the resultant serum was used for the ALT assay. Data are means ± SEM (n = 4). *$p < 0.05$ as compared to the vehicle-treated group.

modification of the surface charge decreased the amount of acute hepatic injury caused by silica nanoparticles.

We then examined the chronic liver injury caused by 60 mg/kg of SP70-C or SP70-N as compared to 30 mg/kg of SP70. Nanoparticles were intravenously injected into mice twice a week for 4 weeks. We assessed the presence of liver fibrosis, because it is a symptom of chronic liver injury. We determined the hepatic hydroxyproline contents in the silica nanoparticle–treated mice (Fig. 4A). SP70, but not SP70-N or SP70-C, significantly increased the hepatic hydroxyproline content by 3.5-fold over the control value. Moreover, collagen, which accumulates in the fibrotic liver, was stained with Azan reagent, and blue-stained regions were observed in SP70-treated, but not SP70-C- and SP70-N-treated, liver sections (Fig. 4B-E). Thus, the chronic administration of SP70-C and SP70-N did not cause hepatic fibrosis in mice.

In this study we found that the surface modification of nanosilica particles with amino group and carboxyl group attenuated liver toxicity. We suspect that this decreased toxicity is due to a decrease in the amount of silica nanoparticles that accumulate in the liver. Oku et al. (1996) reported that the accumulation of liposomes in the liver changed depending on the surface charge of liposomes. Although we confirmed the presence of SP70-N, SP70-C and SP70 in the electron micrograph (data not shown), we were unable to compare the accumulative amounts in the liver. Therefore, an analysis of the accumulative amount of the silica nanoparticles in the liver is necessary in future studies.

The surface charge of nanoparticles might change the pharmacokinetics *in vivo*; for instance, the silica nanoparticles with a positive surface charge have increased paracellular permeability (Lin et al. 2007). Moreover, the phagocytosis of liposomes by hepatic Kupffer cells was promoted by a positive surface charge (Schiestel et al. 2004). We previously reported that the inhibition of phagocytosis by Kupffer cells increased the toxicity of nanosilica particles (Nishimori et al. 2009a). Therefore, it is thought that the nanoparticles with a positive surface charge have decreased hepatic toxicity due to increased phagocytosis by liver Kupffer cells.

This report is the first to indicate that altering the surface charge of nanomaterials changes their toxicity. Further studies based on these data will provide useful information regarding the safety of the nanomaterials.

3. Experimental

3.1. Materials

Silica particles with a diameter of 70 nm were obtained from Micromod Partikeltechnologie GmbH (Rostock, Germany). Silica particles with a diameter of 70 nm that were modified with the amino group or the carboxyl group were obtained from Micromod Partikeltechnologie GmbH (Rostock, Germany). The size distribution of the particles was analyzed using a Zetasizer (Sysmex Co., Kobe, Japan), and the mean diameters were 61.5 and 70.5 nm, respectively. The electric charge of the particles, also measured using the Zetasizer, was found to be –19.7 and –52.4 mV, respectively. The particles were spherical and nonporous and were stored at 25 mg/mL in an aqueous suspension. The suspensions were thoroughly dispersed by sonication before use and then diluted in ultrapure water. All reagents used were of research grade.

3.2. Animals

Eight-week-old BALB/c male mice were purchased from Shimizu Laboratory Supplies Co., Ltd. (Kyoto, Japan) and were maintained in a controlled environment (23 ± 1.5 °C; 12-h light/dark cycle) with access to standard rodent chow and water *ad libitum*. The mice were left to adapt to the new environment for 1 week before commencing with the experiment. Mice that received a single treatment of silica nanoparticles were anesthetized for sacrificing 24 h after intravenous injection. Mice in the frequent treatment group received intravenous administration of silica nanoparticles twice a week for 4 weeks. The experimental protocols conformed to the ethical guidelines of the Graduate School of Pharmaceutical Sciences, Osaka University.

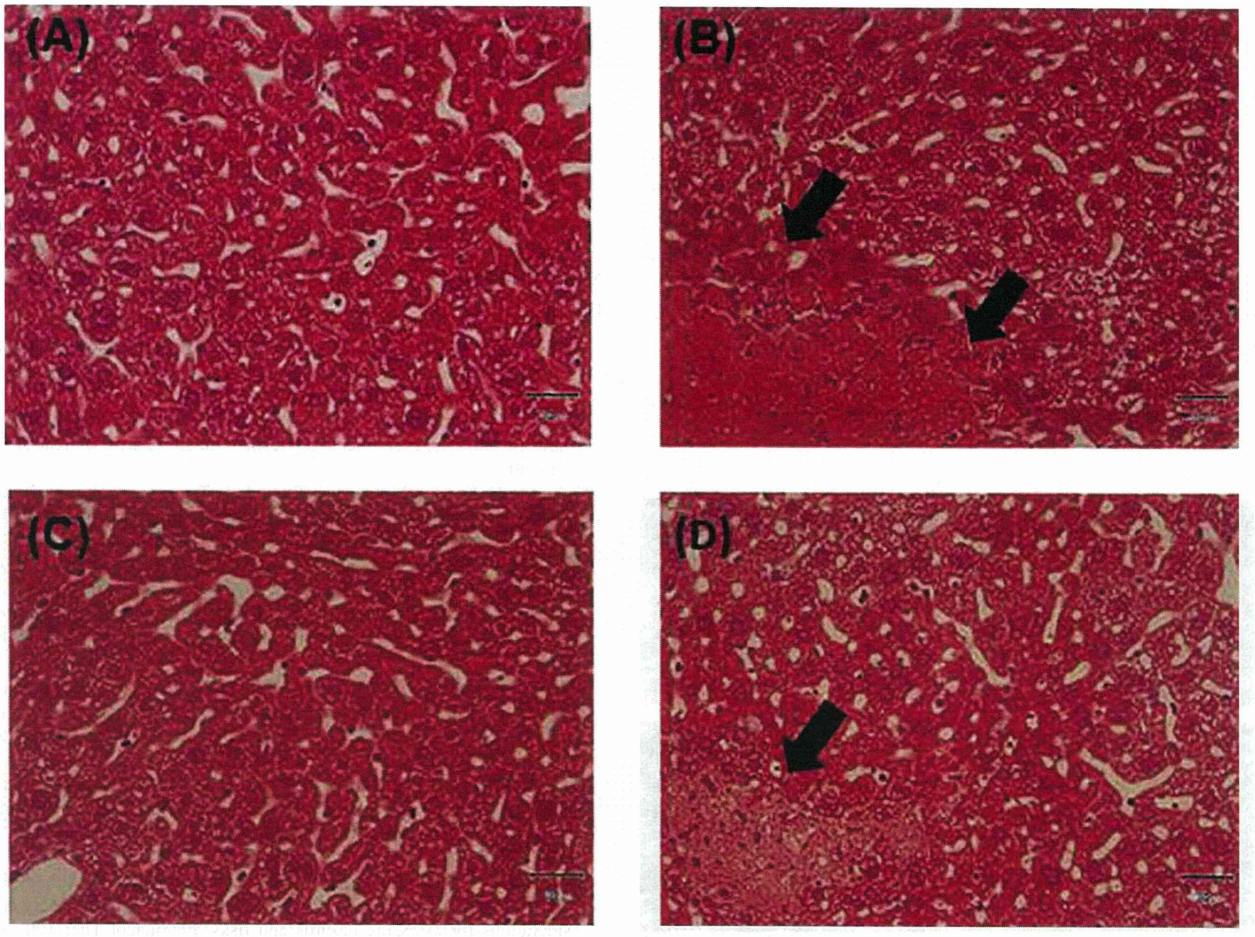

Fig. 2: Hematoxylin and eosin staining of the liver sections. Twenty-four h after administration, the liver was excised from the mice treated with vehicle (A), SP70 (B), SP70-N (C) or SP70-C (D) and fixed with 4% paraformaldehyde. Tissue sections were stained with hematoxylin and eosin and observed under a microscope. The arrows indicate areas of hepatic injury.

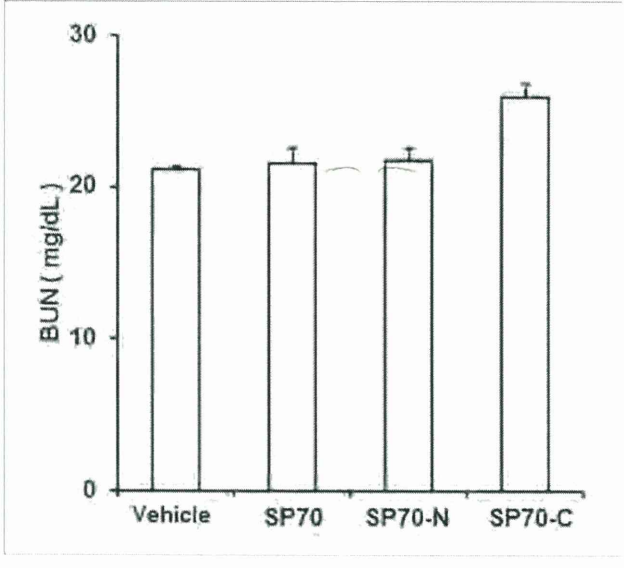

Fig. 3: Effect of SP70-N and SP70-C on kidney. SP70, SP70-N and SP70-C were intravenously administered at 40 mg/kg, 60 mg/kg, and 60 mg/kg, respectively. At 24 h after administration, blood was collected, and the resultant serum was used for the BUN assay with a commercially available kit. Data are means ± SEM (n = 4).

3.3. Biochemical analysis

Serum alanine aminotransferase (ALT) and blood urea nitrogen (BUN) were measured with commercially available kits according to the manufacturer's protocols (Wako Pure Chemical Industries, Osaka, Japan).

3.4. Histological analysis

The liver was excised and fixed with 4% paraformaldehyde. After sectioning, thin tissue sections of tissues were stained with hematoxylin and eosin for histological observation. Liver sections were stained with Azan-Mallory for observation of liver fibrosis.

3.5. Measurement of hydroxyproline content

Hepatic hydroxyproline (HYP) content was measured using Kivirikko's method (Kivirikko et al. 1967), with some modifications. Briefly, liver tissue (50 mg) was hydrolyzed in 6 mol/L HCl at 110 °C for 24 h in a glass test tube. After centrifugation at 3000 rpm for 10 min, 2 mL of the supernatant was neutralized with 8 N KOH. Two grams of KCl and 1 mL of 0.5 mol/L borate buffer were then added to the resultant solution, followed by incubation for 15 min at room temperature and a further incubation for 15 min at 0 °C. Freshly prepared chloramine-T solution was then added and the solution was incubated at 0 °C for 1 h, followed by the addition of 2 mL of 3.6 mol/L sodium thiosulfate. The samples were incubated at 120 °C for 30 min, and then 3 mL toluene was added with incubation for a further 20 min at room temperature. After centrifugation at 2000 rpm for 5 min, 2 mL of the supernatant was added to 0.8 mL of buffer containing Ehrlich's reagent and incubated for 30 min at room temperature. The samples were then transferred to a plastic tube and the absorbance was measured at 560 nm. Hydroxyproline content was expressed as micrograms of hydroxyproline per gram of liver.

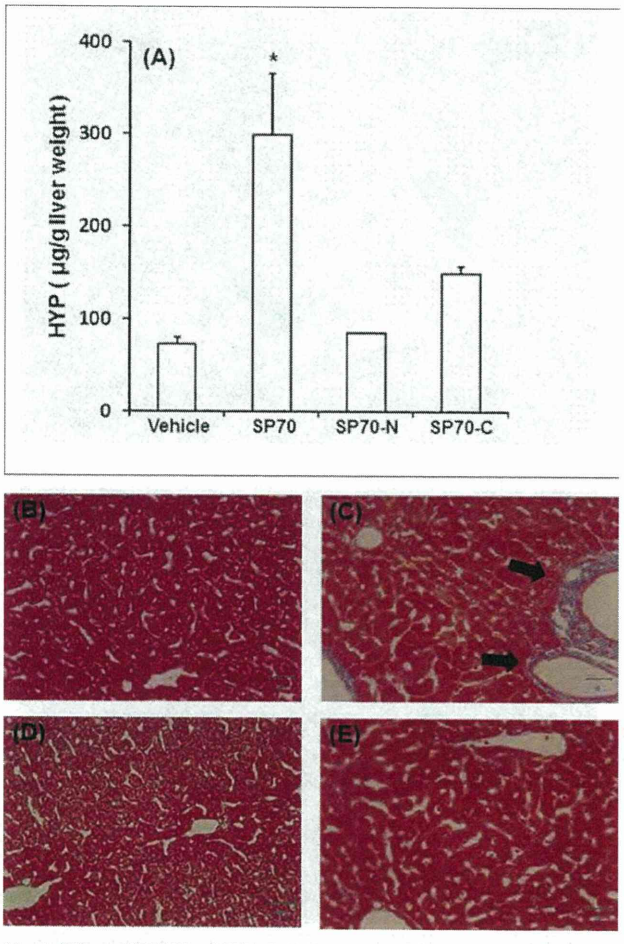

Fig. 4: Effect of SP70-N and SP70-C on chronic liver injury. SP70 was injected into mice every 3 days for 4 weeks at 30 mg/kg. SP70-C and SP70-N was injected into mice every 3 days for 4 weeks at 60 mg/kg. Three days after the last injection, the mice were sacrificed. Hydroxyproline levels (A) in the liver were measured. The liver was excised from mice treated with vehicle (B), SP70 (C), SP70-N (D) or SP70-C (E) and fixed with 4% paraformaldehyde. Tissue sections were stained with Azan and observed under a microscope. The arrows indicate areas of hepatic fibrosis. Data are means ± SEM (n = 4). *$p < 0.05$ as compared to the vehicle-treated group.

3.6. Statistical analysis

The data were analyzed for statistical significance using Dunnett's test. P values less than 0.05 were considered statistically significant.

References

Dobson J (2006) Magnetic micro- and nano-particle-based targeting for drug and gene delivery. Nanomed 1: 31–37.

Kim JS, Yoon TJ, Yu KN, Kim BG., Park SJ, Kim HW, Lee KH, Park SB, Lee JK, Cho MH (2006) Toxicity and tissue distribution of magnetic nanoparticles in mice. Toxicol Sci 89: 338–347.

Kivirikko KI, Laitinen O, Prockop DJ (1967) Modifications of a specific assay for hydroxyproline in urine. Anal Biochem 19: 249–255.

Lin YH, Mi FL, Chen CT, Chang WC, Peng SF, Liang HF, Sung HW (2007) Preparation and characterization of nanoparticles shelled with chitosan for oral insulin delivery. Biomacromolecules 8: 146–152.

Nishimori H, Kondoh M, Isoda K, Tsunoda S, Tsutsumi Y, Yagi K (2009a) Silica nanoparticles as hepatotoxicants. Eur J Pharm Biopharm 72: 496–501.

Nishimori H, Kondoh M, Isoda K, Tsunoda S, Tsutsumi Y, Yagi K (2009b) Histological analysis of 70-nm silica particles-induced chronic toxicity in mice. Eur J Pharm Biopharm 72: 626–629.

Oku N, Tokudome Y, Namba Y, Saito N, Endo M, Hasegawa Y, Kawai M, Tsukada H, Okada, S (1996) Effect of serum protein binding on real-time trafficking of liposomes with different charges analyzed by positron emission tomography. Biochim Biophys Acta 1280: 149–154.

Schiestel T, Brunner H, Tovar G.E (2004) Controlled surface functionalization of silica nanospheres by covalent conjugation reactions and preparation of high density streptavidin nanoparticles. J Nanosci Nanotechnol 4: 504–511.

Smith B, Wepasnick K, Schrote KE, Cho HH, Ball WP, Fairbrother DH (2009) Influence of surface oxides on the colloidal stability of multi-walled carbon nanotubes: a structure-property relationship. Langmuir 25: 9767–9776.

Warheit DB, Sayes CM, Reed KL, Swain KA (2008) Health effects related to nanoparticle exposures: environmental, health and safety considerations for assessing hazards and risks. Pharmacol Ther 120: 35–42.